Transcriptional regulatory framework for vascular cambium development in *Arabidopsis* roots

Jing Zhang[1,2,3], Gugan Eswaran[1,2,11], Juan Alonso-Serra[1,2,11], Melis Kucukoglu[1,2], Jiale Xiang[1,2], Weibing Yang[3], Annakaisa Elo[1,2], Kaisa Nieminen[4], Teddy Damén[1,2], Je-Gun Joung[5,6], Jae-Young Yun[7], Jung-Hun Lee[5], Laura Ragni[8], Pierre B. de Reuille[9], Sebastian E. Ahnert[3,10], Ji-Young Lee[5,*], Ari Pekka Mähönen[1,2,*] and Ykä Helariutta[1,2,3,*]

[1]Institute of Biotechnology, HiLIFE, University of Helsinki, Helsinki 00014, Finland

[2]Organismal and Evolutionary Biology Research Programme, Faculty of Biological and Environmental Sciences, and Viikki Plant Science Centre, University of Helsinki, Helsinki 00014, Finland

[3]The Sainsbury Laboratory, University of Cambridge, Bateman Street, Cambridge CB2 1LR, United Kingdom

[4]Natural Resources Institute Finland (Luke), Production systems, Plant genetics, Viikinkaari 1, FI-00790 Helsinki, Finland

[5]School of Biological Sciences, Seoul National University, 1 Gwanak-ro, Gwanak-gu, Seoul, Korea

[6]Samsung Genome Institute, Samsung Medical Center, Seoul, Korea

[7]Center for Genome Engineering, Institute for Basic Science, Daejeon, Korea

[8]ZMBP-Center for Plant Molecular Biology, University of Tübingen, Auf der Morgenstelle 32, D-72076 Tübingen, Germany

[9]University of Bern, Altenbergrain 21, CH-3013 Bern, Switzerland

[10]Theory of Condensed Matter, Cavendish Laboratory, University of Cambridge, JJ Thomson Avenue, Cambridge CB3 0HE, United Kingdom

[11] These authors contributed equally: Gugan Eswaran, Juan Alonso-Serra

[*]Authors for correspondence: jl924@snu.ac.kr; aripekka.mahonen@helsinki.fi; yrjo.helariutta@slcu.cam.ac.uk

Vascular cambium, a lateral plant meristem is a central producer of woody biomass. Although a few transcription factors (TFs) have been shown to regulate cambial activity[1], the phenotypes of the corresponding loss-of-function mutants are relatively modest, highlighting our limited understanding of the underlying transcriptional regulation. Here, we utilize cambium cell-specific transcript profiling followed by a combination of TF network and genetic analyses to identify 62 novel TF genotypes displaying an array of cambial phenotypes. This approach culminated in virtual loss of cambial activity when both *WUSCHEL-RELATED HOMEOBOX 4* (*WOX4*) and *KNOTTED-like from Arabidopsis thaliana 1* (*KNAT1*; also known as *BREVIPEDICELLUS* (*BP*) were mutated, thereby unlocking the genetic redundancy in the regulation of cambium development. We also identified TFs with dual functions in cambial cell proliferation and xylem differentiation, including *WOX4, SHORT VEGETATIVE PHASE* (*SVP*) and *PETAL LOSS* (*PTL*). Using the TF network information, we combined overexpression of the cambial activator *WOX4* and removal of the putative inhibitor *PTL* to engineer *Arabidopsis* for enhanced radial growth. This line also showed ectopic cambial activity, thus further highlighting the central roles of *WOX4* and *PTL* in cambium development.

Vascular cambium is a secondary meristem which originates from the primary meristems, the shoot apical meristem (SAM) and the root apical meristem (RAM)[2]. In roots, cambium is derived from xylem associated procambium and xylem pole pericycle (XPP) cells[3]. Radial growth involves various processes from cambial cell proliferation (i.e. cambial activity) to the maturation of xylem and phloem. The herbaceous plant *Arabidopsis thaliana* serves as an excellent model to study cambium development because activation and subsequent radial growth can be accurately traced in time[3,4] (Supplementary Fig. 1). It is known that TFs play crucial roles in regulating the maintenance of the SAM and RAM; for example, a single mutation in TF encoding genes, such as

WUSCHEL(*WUS*)[5] or *SHOOT MERISTEMLESS* (*STM*)[6] in the SAM or *SHORT-ROOT* (*SHR*)[7-10] or *SCARECROW* (*SCR*)[7,11] in the RAM, can result in the termination of apical growth. Several TFs have been found to be required for cambial meristematic activity, including *WOX4*[12-14], *WOX14*[15], *AINTEGUMENTA* (*ANT*)[16], *ETHYLENE RESPONSE FACTOR 018*[17] and *ERF109*[17] as well as a set of *AUXIN RESPONSE FACTORS* (*ARFs*)[3,18]. However, only relatively modest proliferation phenotypes were seen in mutants of these genes, even in mutants like *wox4 wox14*[15], *erf018 erf109*[17] or *arf* combinations[3,18]. This indicates a high degree of functional redundancy in the transcriptional regulation of cambial activity.

To identify novel cambium TFs, we performed a genome-wide transcript profiling in *Arabidopsis* roots using Fluorescence-activated cell sorting (FACS) in combination with microarray technology[19] (Fig. 1a), based on procambium and cambium expressing *ARABIDOPSIS RESPONSE REGULATOR 15* (*ARR15*)::GFP (Fig. 1a; Supplementary Fig. 2a). Subsequent meta-analysis including assessment of Differentially Expressed Genes (DEG)[19] and gene regulatory Modules[20,21] predicted 41 TF-encoding genes that were expressed in the cambium (Supplementary Note; Fig. 1a; Supplementary Fig. 2b; Supplementary Tables 1, 2). To experimentally validate the radial expression patterns of the candidate TFs, we examined their transcriptional GUS fusions in early stage (1-2 week) and transcript localization with RNA *in situ* hybridisation in late stage (5-week). This resulted in a list of 32 genes with diverse expression patterns in cambium (Supplementary Table 2), which we considered as "Cambium TFs" in subsequent analyses (Supplementary Note; Fig.1b; Supplementary Fig. 3).

Next, we investigated the effect of individual candidate TFs on cambial activity by generating estradiol inducible overexpression constructs under the 35S promoter[22] in the line expressing a cambial cell proliferation marker line *pCYCD3;1::GUS* (Ler, referred to as CGL hereafter)[16]. Phenotypic characterization of each overexpression line after a 7-day induction suggested that a few TFs were sufficient to control cambial activity. Based on changes in the *pCYCD3;1::GUS* patterns

or in radial growth, we found that *WOX4*, *WOX14*, *NAC DOMAIN CONTAINING PROTEIN 15* (*ANAC015*), *KNAT1* and *LOB DOMAIN-CONTAINING PROTEIN 3* (*LBD3*) promote whereas *SVP*, *RESPONSE TO ABA AND SALT 1* (*RAS1*), *PTL* and *MYB87* inhibit cambial activity. Furthermore, we observed that *LBD4* seems to affect vascular patterning (Supplementary Note; Fig. 2a; Supplementary Fig. 4).

We next selected a subset of 13 cambium TFs which displayed prominent overexpression phenotypes (Fig. 2a) or otherwise represented one of the TF gene families expressed in the cambium (Supplementary Note; Supplementary Table 2) and used these to construct a cambium transcriptional regulatory network. A 24-hour induction of these 13 genes, and the reciprocal Quantitative Reverse Transcription PCR (qRT-PCR) analysis produced a square matrix of their transcriptional interdependence (Supplementary Table 3a, b), which served as the input for the network construction (Methods). A pared-back version of the network was constructed to highlight connections that were more likely to correspond to direct interactions (Methods; Supplementary Note). We took this to be our final network (Fig. 2b). Multiple levels of hierarchical interactions among target TFs were revealed in the network, and several major nodes were identified, including *WOX4*, *KNAT1*, *LBD4* and *PTL*.

We then tested the cambium network experimentally. To this end, we carried out network perturbation analysis (Supplementary Note) to test whether the network could predict the severity of the cambial phenotypes of single and double mutant combinations of the 13 genes (Supplementary Table 3c). Cambial phenotype, that is, vascular "diameter" representing radial growth and "cell count" illustrating cambial cell proliferation (Supplementary Note) correlated well with the prediction (Fig. 2d; Supplementary Fig. 5a), indicating that our network specifically represents cambium regulation. The network analysis guided us to investigate additional combinatorial mutants involving homologous TFs and higher order mutants of the cambium TFs, resulting in roughly 100 genotypes with an array of vascular phenotypes, including the mutants characterized

100 above (Supplementary Note; Fig. 2c; Supplementary Fig. 5). This included 62 novel TF genotypes
101 with cambial phenotypes (Supplementary Note; Supplementary Table 6a).

102 Of the analysed single mutants, the *KNAT1* mutant (referred to as *bp* hereafter) exhibited the
103 greatest reduction in cambial activity (Fig. 3a; Supplementary Table 6a,b). Several other mutants,
104 including *wox4*, *svp* and *ant*, displayed defects in cambial cell proliferation (Fig. 3a; Supplementary
105 Table 6a), while *svp* also showed increased vessel density (Supplementary Note; Supplementary Fig.
106 5c; Supplementary Table 6a). Even though radial growth is reduced in these mutants, meristematic
107 activity is maintained, even in *bp* alleles (Fig. 3a), suggesting functional redundancy within the
108 transcriptional regulation of cambial activity. Next we analysed in detail double or triple mutants of
109 closely homologous genes to examine the redundancy within each TF family. Anatomical
110 characterization revealed functional redundancy within the GRAS, ERF, LBD, Trihelix and MYB
111 families, as certain vascular phenotypes were strengthened by a second mutation (Supplementary
112 Note; Supplementary Fig. 6a,b; Supplementary Table 6a,b); however, antagonistic or epistatic
113 interactions were found in KNOX or MADS family, respectively (Supplementary Fig. 6c;
114 Supplementary Table 6a,b).

115 Furthermore, we characterized a number of combinatorial mutants involving TFs from
116 different families. Inspection of the vascular phenotypes demonstrated genetic interactions between
117 these TF families (Supplementary Note; Fig. 3a; Supplementary Figs. 7-9; Supplementary Table 6).
118 In particular, wox*4*, *wox14*, *myb3r4* and *erf072* enhanced the cambial activity defect of *bp* (Fig. 3a;
119 Supplementary Fig. 7b). Unexpectedly, *ptl-1* partially suppressed *bp* phenotypes, indicating that it
120 might function as an inhibitor of cambial activity (Fig. 3a; Supplementary Figs. 7b, 8d). We also
121 found that *ptl-1 svp-41* had an outstandingly high total vessel number (Supplementary Fig. 5b) with
122 slightly reduced cambial activity (Supplementary Fig. 5a; Supplementary Table 6a), indicating
123 specific, inhibitory roles for *PTL* and *SVP* on vessel production in addition to cambial activity

regulation. Altogether, these data indicate that a number of cambium TFs regulate cambium development in a redundant manner.

Among all the double mutants, *bp wox4* (*bp-9 wox4* and *bp-11 wox4*) consistently demonstrated the most severe defects in cambial cell proliferation (Figs. 2c, 3a; Supplementary Table 6a). We therefore explored the progression of the *bp-9 wox4* phenotype in detail (Supplementary Fig. 8). Cambium initiation seemed normal in *bp-9 wox4*; however, during the transition stage we observed the differentiation defect (i.e. xylem adjacent to phloem) at a higher frequency (6/10) than in either *bp-9* (2/10) or *wox4* (1/10). At later stage, vessel differentiation along the xylem axis was delayed in *bp-9 wox4*, probably due to reduced cambial activity from XPP cells[3]. Importantly, gaps in the vasculature were discovered in 7-week old *bp-9 wox4* plants (Supplementary Fig. 8d), suggesting that cambial activity had been abolished in certain circumferential positions. Therefore, our data support the roles of *KNAT1* and *WOX4* as two master regulators of cambial activity.

Despite the strong phenotype of *bp-9 wox4*, the double mutant displayed residual vascular cambial activity, indicating further redundancy among cambium TFs. Analyses of various higher order mutants showed that only *ant* could slightly enhance the defects in cambial activity in *bp-9 wox4* (Figs. 2c, 3a; Supplementary Table 6a), whereas *ptl-1* suppressed the defects (Supplementary Fig. 9a). When the mutant of *PHLOEM INTERCALATED WITH XYLEM* (*PXY*; also known as *TDIF RECEPTOR* (*TDR*)), the receptor-like kinase acting upstream of WOX4[13,15], was introduced into *bp-9 wox4*, cambial activity was virtually eliminated (Supplementary Fig. 9b). This extreme phenotype indicates the synergistic effect between the *KNAT1*-mediated regulatory pathway and the *PXY-WOX4* pathway and their fundamental roles on cambial activity. Collectively, our systematic phenotypic characterization of combinatorial mutants demonstrated functional redundancy among various TF families in regulating cambial activity and revealed some of the key players and interactions constituting this redundancy.

149 To inspect the potential link between the radial growth phenotypes and changes in gene
150 expression, we used RNA-Seq to examine the whole-genome transcriptome in 12-day old wild-type
151 and selected mutants. Since the two receptor kinases *PXY* and *ER* are known to be important
152 regulators of radial growth[15,23], *pxy er*[15] was included as an additional control of reduced cambial
153 activity (Supplementary Fig. 10). Our analysis showed that the vascular diameter correlated
154 positively with the network prediction and negatively with the number of DEGs (Supplementary
155 Fig. 10c, d). The latter observation suggests that plants with a more severe vascular phenotype had
156 more genes with altered expression. We found that all of the mutants had a much higher proportion
157 of perturbed genes in the cambium enriched genes and our list of 32 cambium TFs than in either the
158 whole transcriptome or in xylem network genes[24] (Fig. 3b; Supplementary Table 8), highlighting
159 the link between the TFs identified in this study and cambium development. The fact that the xylem
160 network was largely interfered in *wox4* reflects the roles of WOX4 in xylem differentiation. We
161 therefore investigated the xylem phenotypes of *wox4* and *bp-9*, the two single mutants exhibiting
162 the strongest cambial phenotypes (Supplementary Fig. 10), using LithoGraphX[25,26], a previously
163 published tool for vascular phenotype quantification (Figs. 3c, d; Supplementary Fig. 11). This
164 analysis showed that the distribution of vessel cell size in *wox4* differed from Col and *bp-9*, and the
165 mean vessel cell size was larger in *wox4* than in Col (Fig. 3c, d). Taken together the cell dimension
166 and transcriptomic data, in addition to its well-known role in regulating cambial cell proliferation,
167 WOX4 may also have a role in xylem vessel expansion. Given that the cells defining the stem cell
168 organizer also possess xylem identity[3], the dual roles of WOX4 suggest that it may regulate stem
169 cell or its organizer function.

170 Previous work has shown that it is possible to influence cambial activity by overexpressing
171 TFs[27,28]. Therefore, we asked whether more prominent radial growth could be achieved by
172 combining multiple positive factors and removing negative factors. First, we made double
173 overexpression (OE) lines by crossing WOX4-OE with other OE lines. The results showed that

cambial activity was significantly increased in WOX4-OE (#6) and all double overexpressing lines compared with WT (CGL) (Fig. 4a; Supplementary Fig. 12). Although the total cell number did not increase further in the double-overexpressors, each overexpressor exerted diverse effects combined with WOX4-OE (Fig.4a; Supplementary Fig. 12). In combination with WOX4-OE (#6), WOX14-OE increased both the number and percentage of cambium cells while ANAC015-OE and KNAT1-OE increased the numbers and percentages of differentiated vessels which are the main source of biomass. Intriguingly, in the double-overexpressors including KNAT1-OE and ANAC015-OE, the cambium domain was narrower and there was less ectopic cell proliferation in the phloem and periderm region, resulting in a more organized pattern, as in WT (Fig. 4a; Supplementary Fig. 12). These data suggest that *WOX14* acts jointly with *WOX4* to promote cambial cell proliferation while *ANAC015* and *KNAT1* might accelerate xylem differentiation in the WOX4-OE background to maintain the balance between cambial cell proliferation and differentiation.

We also combined WOX4-OE and *ptl-1* to test whether cambial activity could be further enhanced when a putative negative factor was removed. The comparison between WOX4-OE (#5) in Col (WOX4-OE_#5;Col) and in *ptl-1* (WOX4-OE_#5;*ptl-1*) demonstrated that cambial activity was significantly enhanced by *ptl* mutation (Fig. 4b). The total cell number in WOX4-OE_#5;*ptl-1* was almost double than in WT (Col) (Supplementary Fig. 13a). Surprisingly, longer-term (4-week) induction of WOX4-OE;*ptl-1* led to the formation of ectopic cambium islands comprising cambium-like cells, vessels and sieve elements in most analysed plants (Fig. 4c; Supplementary Fig. 13e), indicating that in the absence of *PTL*, enables *WOX4* to be sufficient to induce vascular cambium identity. Given that *PTL* is expressed more broadly towards the phloem domain than *WOX4* (Fig. 1b), our data suggest that PTL prevents WOX4 activity in the phloem side.

Our genetic and gene expression data demonstrate that cambium development is orchestrated through a sophisticated transcriptional network involving a large number of TFs. Simultaneous removal of multiple factors resulted in a partial abolishment in cambial activity, indicating that

several pathways mediated by these TFs function redundantly during cambium development. Future studies will uncover whether these TFs interact with the regulators defining the stem cell organiser of the vascular cambium[3] at the cellular level. By combining overexpressors with loss-of-function mutants, we were able to generate transgenic lines with enhanced cambial activity. Since these lines also slightly inhibited apical growth (Supplementary Figs. 12d and 13d), a future challenge is to optimize the genetic engineering of these regulators (for example by using tissue-specific promoters[29-31]) to increase biomass, particularly in woody species.

Methods

Fluorescence-activated cell sorting (FACS) and microarray expression data

The genome-wide transcript profiles in *Arabidopsis* roots have been generated by integration of microarray datasets in the cambium generated in this study (Supplementary Table 1b) and other individual cell types reported previously [19,32-34]. To generate the cambium expression data, about 200 roots of 8-day old seedlings were dissected into three segments (about 1cm per segment) and the basal (ARRI, cambium), middle (ARRII, developing cambium) and apical (ARRIII, procambium) regions were separately collected (Supplementary Fig. 2a). All visible lateral roots were removed with razor blade. Protoplasts from these root segments were isolated and sorted through FACS. RNA transcripts collected from GFP expressing protoplasts were profiled on the Affymetrix ATH1 GeneChips. Parallel profiling was done upon treatment of synthetic cytokinin 6-Benzylaminopurine (BAP) for 48 hours, marked as BAP_ARRI, BAP_ARR II and BAP_ARR III (Supplementary Table 1a). The obtained CEL files (GEO accession number GSE125244) were combined with CEL files for other 17 non-overlapping cell types and normalized using mixed model ANOVA[35]. Genes that are enriched in any of the six ARR15 data compared with non ARR15 data with more than 1.2 fold and False Discovery Rate (FDR) adjusted *P* value (*P*adj) less

than 0.01 were defined as differentially expressed genes (DEGs). 543 DEGs were identified and marked as cambium enriched genes (Supplementary Table 1c).

Gene regulatory module identification

23 non-overlapping cell type specific profiling data were normalized at the probe level using the GC content based robust multi-array algorithm (GCRMA)[36]. The log ratios between each cell type and other non-overlapping cell types using the LIMMA test, which is based on linear models and empirical Bayes methods[37], were calculated. 12,828 genes, which are expressed in at least one cell type with more than 2-fold difference with FDR less than 0.01 were identified and further processed for module identification. To identify regulatory modules, we applied Genomica (http://genomica.weizmann.ac.il), an evolved version of the GeneXPress[38] that clusters the genes and samples simultaneously and build the best regulation programs by learning regression tree using the expression profiles of TFs. This algorithm assumes that TFs regulate gene expression in a combinatorial manner, which likely well reflects TF regulation in higher organisms. 150 modules with predicted gene members (Supplementary Table 1d) were identified, among which 16 showed gene expression patterns highly enriched in the developing cambium and cambium (ARRI/II and/or BAP_ARRI/II). 174 TFs were also identified from the 16 gene modules (Supplementary Table 1e). To find functional enrichment in the identified modules, we extracted significant GO terms in genes belonging to each module using BiNGO Gene Ontology tool, a Cytoscape plugin[39] (http://www.psb.ugent.be/cbd/papers/BiNGO/). The significant GO terms related to biological processes were retrieved by applying hypergeometric distribution and *P*adj less than 0.05 and various GO terms were identified in the cambium enriched gene modules (Supplementary Table 1f)

Plant materials and cloning

All mutants and transcriptional reporter lines analysed in this study were in *Arabidopsis* Columbia (Col) ecotype. Unless otherwise stated, inducible overexpression lines were transformed in

247 *pCYCD3;1::GUS* (Landsberg, referred to as CGL hereafter) [16] background. Seeds published
248 previously were listed in Supplementary table 4b. Mutant alleles purchased from seed stock centre
249 (NASC) or requested were genotyped using primers listed in Supplementary Table 4a.

250 For new transgenic plants, most constructs were generated using Gateway cloning system as
251 described earlier[22]. A two-step PCR amplification protocol was used for all entry clone construction
252 as previously reported[3]. The promoter sequence or coding sequence with stop codes of a candidate
253 gene was amplified from genomic DNA or cDNA from Col roots. For procambium and cambium
254 marker that used for the FACS experiment, the promoter sequence of ARR15 was cloned into
255 pDONR-221 vector and then recombined into Gateway destination vector pMDC204 [40]
256 (https://www.botinst.uzh.ch/en/research/development/grossnik/vectors/MarkdGatewayVectors.html). All gene specific primers and adaptor sequences for cloning were listed in
258 Supplementary Table 4c. For *WOX4* overexpression line construction, genomic fragment containing
259 both exons and introns was amplified from Col DNA. For other genes, only coding sequences were
260 amplified from Col cDNA. For most transcriptional GUS reporter cloning, the promoter sequence
261 was cloned into pDONR-221 entry vector and recombined with pBGWFS7-GFP/GUS (basta
262 selection) or pHGWFS7-GFP/GUS (hygromycin selection) in a single site LR-reaction. For all the
263 overexpression lines and some GUS reporter lines (marked with asterisks in Supplementary Table
264 4c), MultiSite Gateway technology (Invitrogen) was used. Entry clones of *35S::XVE*[22] or candidate
265 promoter (1st box), gene of interest (GOI) or reporter (2nd box) and terminator (3rd box) were
266 combined with destination vector (pBm43GW or pHm43GW) in a MultiSite LR-reaction. For
267 *pLBD4::NYG* cloning, a 4-kb promoter fragment was amplified using primers
268 pLBD4_4kb_XhoI_FW and pLBD4_BamHI_REW and the obtained PCR product was cloned into
269 a destination vector harbouring Nuclear Localization Sequence (NLS) tagged EYFP-GUS, pBI-
270 NYG), using the restriction sites. All generated vectors in this study were listed in Supplementary
271 Table 4c.

Knock-out mutants for *LBD3/ASL9* were generated using CRISPR-CAS9 system. *pJY-35SpCas9-RG1* binary construct was used to target *LBD3/ASL9* via agrobacterium-mediated transformation, in which 35S promoter and AtU6 promoter drive Cas9 and sgRNA, respectively. Three 20-mer targeting regions were selected for CRISPR guide sequences, based on the prediction results from CRISPR RGEN Tools (www.rgenome.net): RG1 (5'-AGACAAAAGGGTCACAGACA-3'); RG2 (5'-TCGCCGGAGAAGTTTACAGC-3'); and RG3 (5'-GGCTCTTTGGCCGGAAAATA -3'). Eight hygromycin-resistant transgenic T1 plants harbouring the CRISPR cassette either with sgRNA-RG1, RG2, or RG3 were grown for T2 germline transmission of potentially edited alleles. Sanger sequencing analyses on targeted regions from T2 progenies revealed that targeted RG1 successfully generated homozygous alleles with an insertion of a single nucleotide "A", thereby leading to a premature stop codons at the 19th codon. This *asl9* mutant was used in this study.

Plant growth and sampling

For surface-sterilization of seeds, two protocols were used in this study. Seeds were surface-sterilized first with 70% ethanol, then in 20% chlorine followed by washing in H2O three times before plating, alternatively seeds were rinsed with 100% ethanol and dried on sterilized filter paper before plating. ½ MS medium with 1% sucrose, 0,5g/L MES pH 5.7-5.8 and 1% Difco agar (BD™) was used in all experiments. Seeds were stratified for two days at 4°C under dark conditions. Seedlings were grown vertically in the growth cabinets (Sanyo) at 22°C under long day conditions (16-hour light and 8-hour dark). The age of the plants was counted from the next day after putting them into the growth cabinets for all experiments. Randomization of plates was carried out every 2-3 days.

For GUS reporter line generation, the corresponding construct was transformed into Col plants and at least two lines with relatively strong signals were analysed for each construct, the similar GUS staining patterns were shown in seedlings at 1-2 week (Fig. 1b, Supplementary Fig. 3).

To generate inducible overexpression lines, all *35S::XVE>>GOI* (GOI-OE was used as short name) constructs were transformed into a cambium marker line CGL[16]. T1 plants were screened based on the changed expression of the cambium marker, *pCYCD3;1::GUS*[16], upon 5µM 17-β-estradiol (est, Sigma) induction. Subsequently, 6-12 independent T1 seedlings for each inducible lines were selected for further investigation. To investigate the vascular phenotypes of each inducible cambial TF, at least two independent T2 or T3 lines with Mendelian segregation were carefully analysed and the most representative images were selected for the Fig. 2a and Supplementary Fig. 4a. Homozygous lines obtained from the same progeny present in Fig. 2a were used for Quantitative Reverse Transcription PCR (qRT-PCR) (Supplementary Table 3a, b) except for WOX4-OE, another line (# 6) was used for qRT-PCR. To produce double overexpression lines, homozygous line of WOX4-OE, # 6 was crossed with homozygous lines of ANAC015-OE, WOX14-OE and KNAT1-OE and obtained F1 seeds were used for further examination. To inspect the effect of WOX4 in *ptl*, WOX4-OE construct was transformed in *ptl-1* (Col) allele and the obtained homozygous lines (#5) were crossed back to both *ptl-1* (referring as WOX4-OE_#5; *ptl-1*) and Col (referring as WOX4-OE_#5; Col) and the F1 plants were used for further study.

For T2 or T3 segregating OE lines (CGL background), transformants were selected from antibiotic plates after 3-4 days and then transferred to a new ½ MS plate for recovery until they were 7-day old. Seedlings with similar growth conditions were then transferred to ½ MS plates containing either 5µM est or an equal volume of DMSO and plants were sampled after 7-day induction. For homozygous or F1 lines, after confirmation the antibiotics resistance on a separate plate, seeds were directly plated on ½ MS before transferring to DMSO or est plates. For most overexpression lines, similar phenotypes were observed in all transformants on estradiol plates. For MYB87-OE, clear segregation of phenotypes was observed after estradiol induction (Fig. 2a) and homozygous plants displayed smaller shoots (Supplementary Fig. 4f), which could be confirmed in the T3 homozygous line.

Genotyping for mutants

Genomic DNA was purified from *Arabidopsis* leaves with either a Whatman FTA classic card method (Sigma-aldrich /Merck) or a precipitation method with Precellys 24 tissue homogenizer (Bertin Technologies) in a buffer containing 3 M Tris-HCl (pH 8.0), 0.5 M EDTA and 3 M NaCl.

For T-DNA insertion lines, genotyping PCR using genomic DNA isolated as described above was carried out to amplify either mutant band or wild-type band using the genotyping primers listed in Supplementary Table 4a. For *ptl-1* and *svp-41*, dCAPs primers were used. For *asl9*, a PCR product flanking the insertion position was amplified and sequenced to identify the mutant allele. All related primers can be found in Supplementary Table 4a. For mutants containing *ant-GK* allele, genotyping was done from the segregation population to identify homozygous plants for further phenotype characterization in each experiment.

Histological analysis and GUS staining

Root samples were collected and vacuum-infiltrated using a fix solution (1% glutaraldehyde, 4% formaldehyde, 0.05M sodium phosphate). After keeping in the fix solution for at least overnight and subsequent ethanol dehydration, the samples were infiltrated and then embedded with Leica basic resin using home-made chambers. 5-µm thin cross sections were cut with a Leica microtome at fixed position in the root (5mm below the hypocotyl-root junction) unless otherwise mentioned and stained with Toluidine blue O or Ruthenium red before imaging. GUS staining and subsequent analysis was performed as previously described[3] with modifications. The collected root samples were vacuum-infiltration with GUS solution for 30min to 1 hour and then incubated at 37°C until the desired level of GUS staining was observed (2 to 16 hours). Fixed and resin (Leica) embedded samples were cut on the microtome into 7-µm sections.

Phenotypic characterization of mutants

A standard procedure was established for mutant phenotype screening as follows. In each experiment, wild-type (Col) and mutants were plated and germinated on ½ MS plates separately as descried above. 5-day old seedlings with similar growth status were transferred to new ½ MS plates. Five or six seedlings were put onto one plate and sampled when they were 17-day old. Randomization of plates was carried out every 2-3 days. Root apical growth was monitored by marking the root tips every 2-3 days until they reached the bottom of the plate. For all analysed mutants, no defect of root apical growth was observed except for *smb-3 brn1-1 brn2-1*. Initially, 10 to 18 seedlings were used for each genotype in each experiment. More plants were used for *ant-GK* combination due to the segregation of the population, for which genotyping PCR was done to identify the homozygous individuals for phenotypic analysis.

Root samples were collected at 17-day, plants with overall growth defects un-related to the genotypes were excluded. Samples were then processed following the histology protocol as described above and obtained cross sections were imaged and analysed. For 6 or 7 week old root phenotype examination, seedling was grown in the pot with soil individually at 23°C under long day conditions in the glass house. Randomization of pots was carried out every 2-3 days.

RNA *in situ* hybridisation

5-week old *Arabidopsis* roots growing in soil under long day conditions in the growth room were harvested and immediately fixed in FAA (3.7% formaldehyde, 5% acetic acid, 50% ethanol) on ice. The samples were embedded in wax and cut into 8-μm sections. The sections were then processed by dewaxing, rehydration and dehydration, as described in the online protocol (http://www.its.caltech.edu/~plantlab/protocols/insitu.pdf). To generate the probes for mRNA *in situ* hybridisation, cDNAs were amplified with gene-specific primers (Supplementary Table 4d) and ligated into the pGEM®-T Easy vector (Promega). The plasmids were verified by sequencing and then used as templates for PCR with the primers T7 and SP6. The PCR products were purified and used for *in vitro* transcription with the DIG RNA Labeling Kit (Roche). Gene-specific probes were

applied onto the sections and hybridisation was performed at 55 °C overnight. After hybridisation, the slices were washed with SSC and incubated with anti-digoxigenin-AP antibody (Roche) for 2 hours at room temperature. Following brief washing with SSC, the signals were detected by overnight colour reaction at 28 °C using NBT/BCIP (Roche). Images were taken with the Zeiss AxioImager M2 microscope fitted with a Zeiss Axiocam MRc colour camera and a PlanApochromat 20x/ 0.8 NA objective. In total, 28 antisense probes were generated in this study and used as cross reference to each other and therefore no sense probe was presented.

qRT-PCR

Inducible overexpression lines for 13 TFs were used for qRT-PCR. T3 homozygous lines were used for most of overexpression lines except that T2 segregating lines were used for ANT-OE and ERF072-OE (Supplementary Table 3a). 8-day old plants were transferred to the plates containing either 5μM est or DMSO control to induce the expression of the target gene for 24 hours. Two third higher part of the primary roots from 20 individual plants were harvested from either est or DMSO plates for RNA purification. For each line, experiment was repeated three times. Total RNA from root samples was isolated with RNeasy Plant Mini Kit (QIAGEN) with an on-column DNase I treatment. cDNA was synthesized using the First Strand cDNA Synthesis Kit (Roche Life Science) according to the manufacturer's instructions. qRT-PCR experiment was performed in 10μl reaction volume using the LightCycler® 480 SYBR Green I Master Mix (Roche Life Science) in a LightCycler® 480 instrument II (Roche Life Science). PCR program was as follows: 95 °C for 5 min, 45 cycles (95 °C for 10s, 60 °C for 10s, 72 °C for 10s), melting curve analysis. Each sample was analysed with three technical replicates. Detected expression levels were normalized using the Comparative CT Method (ΔΔCT method)[41] using multiple reference genes (ACTIN 2, PP2AA3, TIP41, and UBQ 10). All statistical analyses (unpaired parametric t-test) were performed using GraphPad PRISM v.7 (GraphPad Software). All primers used for qRT-PCR are listed in Supplementary Table 4e. Relative expression level (fold change) and significance values were

calculated based on the three independent analyses and put in in the form of a matrix for the subsequent network analysis (See below).

Transcriptional regulatory network construction

The matrix of fold change obtained from qRT-PCR data (Supplementary Table 3a) together with the matrix of *P* value (Supplementary Table 3b) collected from 24-hour induction in the overexpression lines formed the basis of the network construction. We denoted the fold change matrix as F and the significance matrix of *P* values as P, then the directed, signed adjacency matrix A of the network was given by $a_{ij} = 1$ if $f_{ij} > 1$ and $p_{ij} \leq 0.05$, $a_{ij} = -1$ if $f_{ij} < 1$ and $p_{ij} \leq 0.05$ and $a_{ij} = 0$ if $p_{ij} > 0.05$. For the pared-back network, we removed all directed connections between two nodes if a directed path of length between those two nodes exists, with the same overall significance. Hence a direct inhibitory link from gene A to gene B would be removed if there was an activatory link from gene A to another gene C, and an inhibitory link from gene C to gene B (or an inhibitory link from A to C, and an activatory one from C to B). Links were only removed if they do not cut off nodes entirely, which can happen if a connection is both part of a direct and an indirect path.

Network perturbation analysis

The network perturbation analysis was undertaken by measuring the fraction "f" of directed network paths that exist in a network, out of the maximum of N (N-1) directed paths that could possibly exist in a directed network with N nodes. The value of "f" was defined as "Fraction of directed paths measurement". We calculate this value of "f" for the network described above (wild-type) as well as for alternative versions of the same network with single or double knockouts, where we implement a knockout by removing all interactions of the knocked out gene(s). The deviation in the value of "f" between a knockout network and the full network in the wild-type is a measurement of the disruption caused by that knockout in terms of the network topology.

The code for network construction and perturbation analysis can be found on Github (https://github.com/Zhangcambium2019/Zhang2019).

Microscope image processing

To check the expression of *pARR15::GFP* in *Arabidopsis* root, the 8-day old seedling were imaged with Leica SP5 confocal microscopy. To examine the radial patter of *pARR15::GFP*, vibratome sectioning was carried out as previously described[3] and 200-µm sections taken from three positions in the root of the 8-day old seedling (Supplementary Fig. 2a) were cleared with ClearSee solution and stained with 1µg/ml Calcofluor white (Sigma) to visualize the cell wall as reported[3]. Confocal images were acquired with the Leica LAS AF Software.

Images of resin embedded histological cross sections were taken with Leica 2500 or Zeiss Axioimager M2 with 10×, 20× or 40× objectives. The quantification of diameter, area, cell count was done using Fiji (1.0)/ImageJ (1.47v) or LithoGrapX (described later) for specific analysis.

Vascular phenotype quantification with LithoGraphX

LithoGraphX 1.2.2 with the Builder 1.2.2.7 (http://www.lithographx.com/) was employed to analyse the specified experiments following the protocol described earlier[25] with modification. Images were pre-processed in Fiji (1.0)/ImageJ (1.47v) to meet the requirement of LithoGraphX. The details of parameters used in the segmentation pipeline can be found on Github (https://github.com/Zhangcambium2019/Zhang2019). The raw segmentation and measurement data were included in Supplementary Dataset 3. All quantification was restricted to the vasculature so that periderm was excluded (Fig. 4c). The number of all vascular cells, number of vessels and the area of each cell (cell size) was measured with the program and a heatmap was generated based on the size of each cell (Fig. 4c). The “total vascular area” was calculated by making the sum of cell

area of all vascular cells, therefore intercellular spaces were excluded. The number of independent roots for analysis was denoted as "*n*" and the number of cells was denoted as "n_n".

Plots and statistical analysis

Statistical analyses were carried out in SPSS Statistics 24 and R 3.5.1 (http://www.r-project.org/). Bar plots and scatter plots were generated with Microsoft Excel and all other plots were generated with necessary packages using RStudio (1.1.423). All the box-and-whisker plot were created using standard settings 'geom_boxplot' using ggplot2 (3.1.0) package. The median splits first and third quartiles; whiskers extend about 1.5 interquartile range beyond the box and the black dots represent outliers. The half-violin plot is made by combining raw data with violin plot splitting each category in two location. The black dot with whisker indicates the mean value. The related codes can be found on Github (https://gist.github.com/jbburant/b3bd4961f3f5b03aeb542ed33a8fe062 and https://gist.github.com/dgrtwo/eb7750e74997891d7c20).

For large scale characterization of mutants, a two-tailed Student's t-test was carried out using the normalized values to calculate *P* value. The number of independent roots in each experiment was indicated as "*n*" (Supplementary Table 6b) while the total number of roots from the pools of all experiments was denoted as "*N*" (Supplementary Table 6a). The pooled normalized data from all the experiments used to generate the box-and-whisker plot for each genotype. One-way ANOVA analysis was done in SPSS Statistics 24, multiple comparisons were performed using Post-hoc tests Tuckey HSD (for variables with homogenous variance) and Games-Howell (for variables with non-homogenous variance). Homogeneity of variance was defined by Levene's Test. All ANOVA results were included in Supplementary Dataset 2.

RNA-seq profiling and data analysis

For RNA-seq experiment, main root fragments (1 mm to 20 mm below root-hypocotyl junction) of 12-day old plants, including wild-type (Col), *ptl-1*, *asl9*, *svp-41*, *wox4*, *bp-9*, *bp-9 ptl-1*, *bp-9 wox4*

and *pxy er*, undergoing radial growth were collected from 30-60 seedlings depending on the genotype. Visible lateral roots were excised with razor blades. The radial growth status was checked and quantified at the middle position (10mm) of the root fragments used for profiling. For each genotype, three independent replicates were collected. Total RNA was isolated with RNeasy Plant Mini Kit (QIAGEN) with an on-column DNase I treatment. RNA concentration was measured with Qubit® 2.0 Fluorometer together with Qubit RNA BR Assay Kit while the RNA purity was assessed with NanoDrop™ 1000 Spectrophotometer (ThermoFisher Scientific). RNA integrity was assess with RNA integrity number equivalent (RIN^e) using Agilent 2200 TapeStation system following the manufacturer's instructions. RNA samples giving a RIN^e>9 were sent for downstream processing. Library preparation with NEB Next® Ultra™ RNA Library Prep Kit and subsequent sequencing with Illumina HiSeq PE150 (pair-end sequencing) platform were performed by Novogene (China, https://en.novogene.com/). Data Quality Control, Data Filtering, Mapping to Reference Genome, Expression Quantification and DEGs identification were carried out using pipelines from Novogene. TopHat2 algorithm was used for mapping sequence to *Arabidopsis* reference genome (TAIR10). HTSeq software was used to analyse the gene expression levels (read_counts) using the union mode. After normalization, the relative expression (fold change) of one gene was obtained by comparing the average read_counts in each mutant against that in Col with DESeq. Genes with more than 1.5 fold change and *P*adj less than 0.05 was defined as DEGs (Supplementary Table 7). Venn Diagram was generated using Venny 2.1.0 (http://bioinfogp.cnb.csic.es/tools/venny/index.html). All raw data (FASTQ) can be found in NCBI (BioProject ID: PRJNA523600) and normalized read_counts for all samples can be found in Supplementary Dataset 4.

Code availability

Codes for network construction and LithoGraphX analysis can be found on Github (https://github.com/Zhangcambium2019/Zhang2019). R-codes for Boxplot, Half Violin Plot, Median calculation, Average calculation and *P* value calculation can also be found on Github.

Data availability

Gene accession numbers are as follows: *ARR15*, AT1G74890; *CYCD3;1*, AT4G34160; *ANT*, AT4G37750; *WOX14*, AT1G20700; *KNAT1* (also known as *BP*), AT4G08150; *PTL*, AT5G03680; *SVP*, AT2G22540; *AGL24*, AT4G24540; *LBD4*, AT1G31320; *SCL7*, AT3G50650; *AGL14*, AT4G11880; *ATHB53*, AT5G66700; *ATHB5*, AT5G65310; *WRI3*, AT1G16060; *AHL11*, AT3G61310; *MYB47*, AT1G18710; *MYB95*, AT1G74430; *MYB87*, AT4G37780; *STY2*, AT4G36260; *RAS1*, AT1G09950; *AtERF019*, AT1G22810; *AtERF021*, AT1G71450; *AtERF029*, AT4G25490; *AtERF032*, AT1G63030; *AtERF043*, AT4G32800; *AtERF071*, AT2G47520; *AtERF072*, AT3G16770; *WOX4*, AT1G46480; *WOX13*, AT4G35550; *STM*, AT1G62360; *KNAT2*, AT1G70510; *KNAT6*, AT1G23380; *BOP1*, AT3G57130; *BOP2*, AT2G41370; *EDA31*, AT3G10000; *LBD3* (also known as *ASL9*), AT1G16530; *LBD1*, AT1G07900; *SCL4*, AT5G66770; *SCL3*, AT1G50420; *SCL28*, AT1G63100; *ANAC015* (also known as *BRN1*), AT1G33280; *ANAC070* (also known as *BRN2*), AT4G10350; *SMB*, AT1G79580; *ANAC042* (also known as *JUNGBRUNNEN 1*), AT2G43000; *ANAC042-like*, AT3G12910; *MYB3R4*, AT5G11510; *MYB3R1*, AT4G32730; *PXY* (also known as *TDR*), AT5G61480; *ERECTA/ER*, AT2G26330. Raw data of Affymetrix ATH1 GeneChip and RNA-seq data can be found in NCBI as described above. Source data related to LithoGraphX analysis (Fig. 3c, d; Supplementary Fig. 11) and ANOVA analysis (Fig. 4d; Supplementary Figs. 8e, 11, 12, 13) can be found in Supplementary Datasets. The data that support the findings of this study are available from the corresponding author upon request.

References

1. Zhang, J., Nieminen, K., Serra, J.A.A. & Helariutta, Y. The formation of wood and its control. *Current Opinion in Plant Biology* **17**, 56-63 (2014).

2. Nieminen, K., Blomster, T., Helariutta, Y. & Mahonen, A.P. Vascular Cambium Development. *Arabidopsis Book* **13**, e0177 (2015).
3. Smetana, O. *et al.* High levels of auxin signalling define the stem-cell organizer of the vascular cambium. *Nature* **565**, 485-489 (2019).
4. Zhang, J., Elo, A. & Helariutta, Y. Arabidopsis as a model for wood formation. *Current Opinion in Biotechnology* **22**, 293-299 (2011).
5. Laux, T., Mayer, K.F.X., Berger, J. & Jurgens, G. The WUSCHEL gene is required for shoot and floral meristem integrity in Arabidopsis. *Development* **122**, 87-96 (1996).
6. Clark, S.E., Jacobsen, S.E., Levin, J.Z. & Meyerowitz, E.M. The CLAVATA and SHOOT MERISTEMLESS loci competitively regulate meristem activity in Arabidopsis. *Development* **122**, 1567-1575 (1996).
7. Benfey, P.N. *et al.* Root development in Arabidopsis: four mutants with dramatically altered root morphogenesis. *Development* **119**, 57-70 (1993).
8. Helariutta, Y. *et al.* The SHORT-ROOT gene controls radial patterning of the Arabidopsis root through radial signaling. *Cell* **101**, 555-67 (2000).
9. Lucas, M. *et al.* SHORT-ROOT Regulates Primary, Lateral, and Adventitious Root Development in Arabidopsis. *Plant Physiology* **155**, 384-398 (2011).
10. Scheres, B. *et al.* Mutations Affecting the Radial Organization of the Arabidopsis Root Display Specific Defects Throughout the Embryonic Axis. *Development* **121**, 53-62 (1995).
11. DiLaurenzio, L. *et al.* The SCARECROW gene regulates an asymmetric cell division that is essential for generating the radial organization of the Arabidopsis root. *Cell* **86**, 423-433 (1996).
12. Ji, J.B. *et al.* WOX4 Promotes Procambial Development. *Plant Physiology* **152**, 1346-1356 (2010).
13. Hirakawa, Y., Kondo, Y. & Fukuda, H. TDIF Peptide Signaling Regulates Vascular Stem Cell Proliferation via the WOX4 Homeobox Gene in Arabidopsis. *Plant Cell* **22**, 2618-2629 (2010).
14. Suer, S., Agusti, J., Sanchez, P., Schwarz, M. & Greb, T. WOX4 Imparts Auxin Responsiveness to Cambium Cells in Arabidopsis. *Plant Cell* **23**, 3247-3259 (2011).
15. Etchells, J.P., Provost, C.M., Mishra, L. & Turner, S.R. WOX4 and WOX14 act downstream of the PXY receptor kinase to regulate plant vascular proliferation independently of any role in vascular organisation. *Development* **140**, 2224-2234 (2013).
16. Randall, R.S. *et al.* AINTEGUMENTA and the D-type cyclin CYCD3;1 regulate root secondary growth and respond to cytokinins. *Biology Open* **4**, 1229-1236 (2015).
17. Etchells, J.P., Provost, C.M. & Turner, S.R. Plant Vascular Cell Division Is Maintained by an Interaction between PXY and Ethylene Signalling. *Plos Genetics* **8**(2012).
18. Brackmann, K. *et al.* Spatial specificity of auxin responses coordinates wood formation. *Nature Communications* **9**(2018).
19. Birnbaum, K. *et al.* Cell type-specific expression profiting in plants via cell sorting of protoplasts from fluorescent reporter lines. *Nature Methods* **2**, 615-619 (2005).
20. Wagner, G.P., Pavlicev, M. & Cheverud, J.M. The road to modularity. *Nat Rev Genet* **8**, 921-31 (2007).
21. Wang, X.W., Dalkic, E., Wu, M. & Chan, C. Gene module level analysis: identification to networks and dynamics. *Current Opinion in Biotechnology* **19**, 482-491 (2008).
22. Siligato, R. *et al.* MultiSite Gateway-Compatible Cell Type-Specific Gene-Inducible System for Plants. *Plant Physiology* **170**, 627-641 (2016).
23. Uchida, N. & Tasaka, M. Regulation of plant vascular stem cells by endodermis-derived EPFL-family peptide hormones and phloem-expressed ERECTA-family receptor kinases. *Journal of Experimental Botany* **64**, 5335-5343 (2013).
24. Taylor-Teeples, M. *et al.* An Arabidopsis gene regulatory network for secondary cell wall synthesis. *Nature* **517**, 571-U307 (2015).
25. Wunderling, A., Ben Targem, M., de Reuille, P.B. & Ragni, L. Novel tools for quantifying secondary growth. *Journal of Experimental Botany* **68**, 89-95 (2017).
26. de Reuille P.B., R.L. Vascular Morphodynamics During Secondary Growth. in *Xylem. Methods in Molecular Biology* (ed. de Lucas M., E.J.) 103-125 (Humana Press, New York, NY, 2017).
27. Guo, Y., Qin, G.J., Gu, H.Y. & Qu, L.J. Dof5.6/HCA2, a Dof Transcription Factor Gene, Regulates Interfascicular Cambium Formation and Vascular Tissue Development in Arabidopsis. *Plant Cell* **21**, 3518-3534 (2009).

28. Yordanov, Y.S., Regan, S. & Busov, V. Members of the LATERAL ORGAN BOUNDARIES DOMAIN Transcription Factor Family Are Involved in the Regulation of Secondary Growth in Populus. *Plant Cell* **22**, 3662-3677 (2010).
29. Etchells, J.P., Mishra, L.S., Kumar, M., Campbell, L. & Turner, S.R. Wood Formation in Trees Is Increased by Manipulating PXY-Regulated Cell Division. *Current Biology* **25**, 1050-1055 (2015).
30. Zhang, J., Serra, J.A.A. & Helariutta, Y. Wood development: Growth through knowledge. *Nature Plants* **1**, 15060 (2015).
31. Immanen, J. *et al.* Cytokinin and Auxin Display Distinct but Interconnected Distribution and Signaling Profiles to Stimulate Cambial Activity. *Current Biology* **26**, 1990-1997 (2016).
32. Brady, S.M. et al. A high-resolution root spatiotemporal map reveals dominant expression patterns. *Science* **318**, 801-806 (2007).
33. Nawy, T. et al. Transcriptional profile of the Arabidopsis root quiescent center. *Plant Cell* **17**, 1908-1925 (2005).
34. Lee, J.Y. et al. Transcriptional and posttranscriptional regulation of transcription factor expression in Arabidopsis roots. *Proceedings of the National Academy of Sciences of the United States of America* **103**, 6055-6060 (2006).
35. Levesque, M.P. et al. Whole-genome analysis of the SHORT-ROOT developmental pathway in Arabidopsis (vol 4, pg 739, 2006). *Plos Biology* **4**, 1284-1284 (2006).
36. Wu, Z.J., Irizarry, R.A., Gentleman, R., Martinez-Murillo, F. & Spencer, F. A model-based background adjustment for oligonucleotide expression arrays. *Journal of the American Statistical Association* **99**, 909-917 (2004).
37. Smyth, G.K. Limma: linear models for microarray data. in *Bioinformatics and computational biology solutions using R and Bioconductor* 397-420 (Springer, 2005).
38. Segal, E. et al. Module networks: identifying regulatory modules and their condition-specific regulators from gene expression data. *Nature Genetics* **34**, 166-176 (2003).
39. Maere, S., Heymans, K. & Kuiper, M. BiNGO: a Cytoscape plugin to assess overrepresentation of Gene Ontology categories in Biological Networks. *Bioinformatics* **21**, 3448-3449 (2005).
40. Curtis, M.D. & Grossniklaus, U. A gateway cloning vector set for high-throughput functional analysis of genes in planta. *Plant Physiology* **133**, 462-469 (2003).
41. Livak, K.J. & Schmittgen, T.D. Analysis of relative gene expression data using real-time quantitative PCR and the 2(T)(-Delta Delta C) method. *Methods* **25**, 402-408 (2001).

Corresponding authors

Correspondence to Ji-Young Lee: jl924@snu.ac.kr; Ari Pekka Mähönen:

aripekka.mahonen@helsinki.fi; Ykä Helariutta: yrjo.helariutta@slcu.cam.ac.uk.

Acknowledgments

We thank O. Smetana for providing the root cross section sketches for making vector images in Fig. 1a; S. Miyashima for providing the pBI-nlsYFP-GUS vector for the cloning of *pLBD4::nYFP-GUS*; H. Fukuda, J. Murray, D. Smyth, U. Fischer, H. Yu, T. Mizuno, J. Lim, B. Scheres, M. Ito, S. Hepworth, V. Pautot, M. Kater and S. Turner for providing published seeds (Supplementary Table

4a, b); K. Kainulainen and M. Herpola for technical assistance; O. Smetana and L-L. Ye for providing help on finalizing the figures; S. El-Showk for language correction. This work was supported by Finnish Centre of Excellence in Molecular Biology of Primary Producers (Academy of Finland CoE program 2014-2019) decision #271832, the Gatsby Foundation (GAT3395/PR3)), the University of Helsinki (award 799992091) and the European Research Council Advanced Investigator Grant SYMDEV (No. 323052) to Y.H.; Academy of Finland (grants #132376, #266431, #271832), University of Helsinki HiLIFE fellowship to A.P.M.; National Research Foundation of Korea (2018R1A5A1023599 and 2016R1A2B2015258) to J-Y. L.

Author contributions

J.Z., J-Y.L., A.P.M. and Y.H. designed the experiments. J.Z. carried out most of the experiments with the help of other co-authors. K.N. constructed the *pARR15::GFP* line for FACS. K.N., A.E. and J-Y. L. performed FACS and microarray hybridisation. J-Y. L. and J-G. J. analysed the microarray data from the FACS. J.Z. generated and analysed all transgenic lines with input from A.E. on GUS reporter lines. W.Y. and J.Z. did the RNA *in situ* analysis. M.K. conducted the qRT-PCR and analysed the data for network construction. S.E.A constructed the network and carried out perturbation analysis. J.Z. and G.E. generated combinatorial mutants. J-Y. Y. and J-H. L. produced the *asl9* CRISPR mutant. J.Z., G.E., J.X. and T.D. performed mutant genotyping. J.Z. characterized the mutant and overexpression line phenotypes with the assistance from J.X., G.E. and J.A-S. For phenotypic examination of mutants and overexpression lines, J.Z., G.E. and J.A-S conducted quantification and statistical analyses. J. A-S ran the LithoGraphX analysis with input from G.E., L.R. and P.B.R. J.Z. performed the RNA-seq experiment and analysed the RNA-seq data with S.E.A. G.E. drew all box plot figures. J.Z., J-Y.L., A.P.M. and Y.H. wrote the manuscript with the help of co-authors. All authors read and commented on the manuscript.

Competing Interests statement

The authors declare no competing interests.

Figure Legends

Fig. 1 | Identification and validation of cambium transcription factors (TFs) during radial growth in Arabidopsis roots. a, Schematic workflow for the discovery of "cambium TFs". Cells marked by *pARR15::GFP* were isolated from roots at three stages of cambium development and used for genome-wide transcript profiling. Candidate cambium TFs were selected based on the "meta-analysis": an initial 25 TFs were identified based on a combination of two bioinformatic methods, Differentially Expressed Genes (DEG) and Module analysis (shown as Venn diagram), followed by an analysis which added homologues of the initial TFs and cytokinin-induced TFs to obtain a candidate list of 41 TFs (**Supplementary Note**; **Supplementary Table 2**). After experimental validation (shown in **b**), the list of 32 "cambium TFs" were obtained. **b,** Radial expression patterns of a subset of cambium TFs. Cross sections of the transcriptional GUS reporter line in 1-2 week old roots (left) and RNA *in situ* hybridisation in 5-week old roots (right) were displayed are shown for each gene. The primary xylem axis is marked in red on the GUS sections. Black arrow-heads indicate the *in situ* signals. In *pLBD4::nYFP-GUS*, nYFP-GUS refers to Nuclear Localization Sequence tagged eYFP-GUS. All GUS staining was repeated at least three times with similar results. For *in situ* hybridisation, at least 10 Col (wild type) plants were examined for each gene with similar patterns. Scale bars, 100μm.

Fig. 2 | A transcriptional network based on inducible overexpression analysis largely predicts the severity of cambial loss-of-function mutants. a, Inducible overexpression of certain cambium transcription factors (TFs) affected cambial activity. Cross sections of GUS stained followed by

659 Ruthenium red contrast stained roots of control (DMSO) and 5μM estradiol (est) treated plants from
660 overexpression (OE) lines. Each gene was induced for 7 days in 7-day old seedlings. All lines were
661 generated in a cambial cell proliferation marker line *pCYCD3,1::GUS* (Ler) background. The GUS
662 signal intensity represents the change in the expression level of *CYCD3;1*. Control sections from all
663 OE lines showed similar GUS patterns, and only the DMSO section from WOX4-OE is shown.
664 Phenotypes were characterized in T2 or T3 segregating lines, and similar results were found in at
665 least two independent lines (See Methods for details). Segregation of the phenotype was observed
666 in MYB87-OE. "hemi" refers to hemizygous plants; "hm" refers to homozygous plants. The
667 primary xylem axis is marked in red. Scale bars, 100μm. **b,** The transcriptional regulatory network
668 was constructed based on quantitative Reverse Transcription PCR (qRT-PCR) analysis in inducible
669 overexpression lines of thirteen selected transcription factors (**Supplementary Table 3a** and **b**).
670 Positive and negative regulation are shown as arrow-headed line and bar-headed lines, respectively.
671 The width of the line indicates the strength of the regulation. **c,** An array of vascular phenotype
672 (vascular diameter) was displayed among wild-type (Col) and all mutants characterized at 17-days
673 under long day conditions. Data were collected from a number of independent experiments, and
674 phenotype data for each mutant were normalized to the Col within the same analysis. Box-and-
675 whisker plots are centred at the median, which splits first and third quartiles. Whiskers show range
676 and black dots represent outliers. For each genotype, the median of vascular diameter, the frequency
677 of significance (examined by a two-tailed Student's t-test in each experiment) observed in multiple
678 experiments and the exact total number of independent roots (N) were listed in **Supplementary**
679 **Table 6a**. **d,** The correlation between the phenotype severities predicted by the network (indicated
680 as "Fraction of directed paths measurement") (**Supplementary Table 3c**) and the observed
681 phenotype (Normalized vascular diameter, **Supplementary Table 6a**) for Col and related single
682 and double mutants. Linear regression model was adopted and R-squared (R^2) was used to measure
683 the correlation. The genotypes used in the analysis was listed in **Supplementary Dataset 1** and the

exact total number of independent roots (N) for each genotype was listed in **Supplementary Table 6a**.

Fig. 3 | Among the studied TFs, *WOX4* and *KNAT1* emerged as major regulators of radial growth. a, Toluidine blue O-stained cross sections of roots of 17-day old wild-type (Col) and various mutants displaying radial growth defects. Red dots indicate cambium cells. The primary xylem axis is marked in red. For each genotype, the exact number of independent experiments and the number of roots in each experiment was listed in **Supplementary Table 6a**. Scale bars, 50μm. **b,** The overlapping genes between Differentiated Expressed Genes (DEGs) identified by RNA-Seq profiling and all *Arabidopsis* genes (TAIR10), Cambium enriched genes (**Supplemental Table 1c**), Cambium transcription factors (TFs) (**Supplementary Table 2**) and xylem network genes (**Supplemental Table 8b**) were obtained by Venn Diagram. The percentage of overlapping genes against all gene lists was calculated and compared in each mutant (**Supplemental Table 8a**). **c,** Characterization of radial growth phenotypes in 17-day old Col, *wox4* and *bp-9* using LithoGraphX. A cell-size heatmap is overlaid on its original greyscale microscopic cross section. The colour scale represents the size of vascular cells. The experiment was repeated twice. n, independent roots. Scale bars, 100μm. **d,** A half-violin plot showing the cell size distribution of differentiated vessels characterized by LithoGraphX. The black dot with lines represents the mean value with confidence interval. Normality was assessed with the Shapiro-Wilk test. Nd, normally distributed; NNd, non-normally distributed; "n_n" indicated the number of all cells analysed. Different letters indicate a significant difference ($P<0.05$) based on a one-way ANOVA (the exact *P* value for each comparison can be found in **Supplementary Dataset 2a**).

Fig. 4 | Activation of positive transcriptional regulators and removal of negative regulator synergistically stimulate cambial activity. a, Cross sections of GUS stained followed by Ruthenium red contrast stained roots from wild-type (cambial cell proliferation marker line *pCYCD3,1::GUS* (Ler), marked as WT (Ler)), *WOX4* single overexpression (OE) line (#6) and three double OE lines. All lines were treated with 5μM estradiol (est) to induce the expression of *WOX4* and co-expression of *WOX4* and *WOX14*, *ANAC015* or *KNAT1* respectively for 7 days in 7-day old seedlings. Phenotypes checked in F1 lines from two independent crosses produced similar results. **b,** Cross sections of Ruthenium red stained roots of wild-type (Col, marked as WT (Col)), WOX4-OE in the Col background (WOX4-OE_#5; Col) and in the *ptl-1* background (WOX4-OE_#5; *ptl-1*). All lines were treated with 5μM est to induce the expression of *WOX4* for 7 days in 10-day old seedlings. Phenotypes analysed in F1 lines from two independent crosses produced similar results. The exact number of independent roots (n) for each line in **a** and **b** can be found in **Supplementary Table 5b**. **c**, Ectopic cambium islands were observed at a high frequency (6/8) in the roots of WOX4-OE_#5*; ptl-1* upon long-term induction but not in WOX4-OE_#5; Col. The expression of *WOX4* was induced for 4-week upon 5μM est treatment. DMSO was used as control. Sections were taken from the main roots 5mm below hypocotyl-root junction. The experiment was repeated twice. The primary xylem axis is marked in red. Scale bars, 100μm.

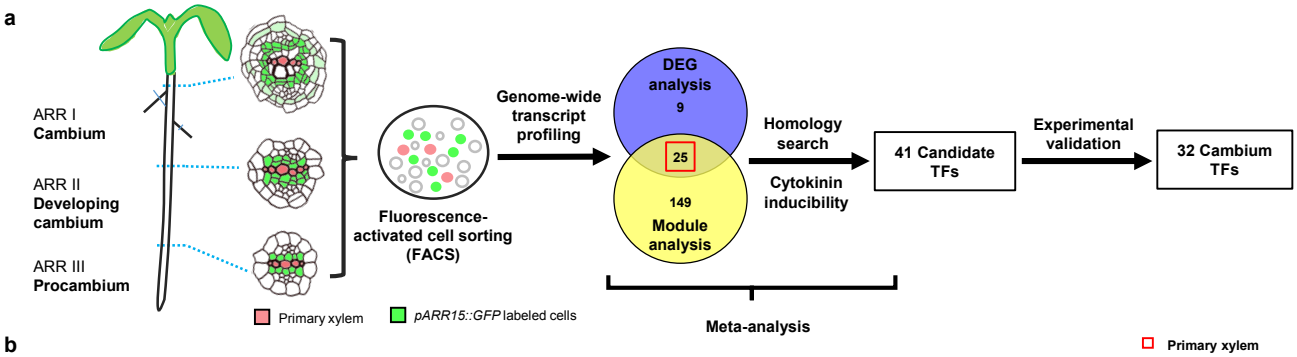
a
ARR I
Cambium
ARR II
Developing
cambium
ARR III
Procambium
Primary xylem
pARR15::GFP labeled cells
Fluorescence-
activated cell sorting
(FACS)
Genome-wide
transcript
profiling
DEG
analysis
9
25
149
Module
analysis
Meta-analysis
Homology
search
Cytokinin
inducibility
41 Candidate
TFs
Experimental
validation
32 Cambium
TFs

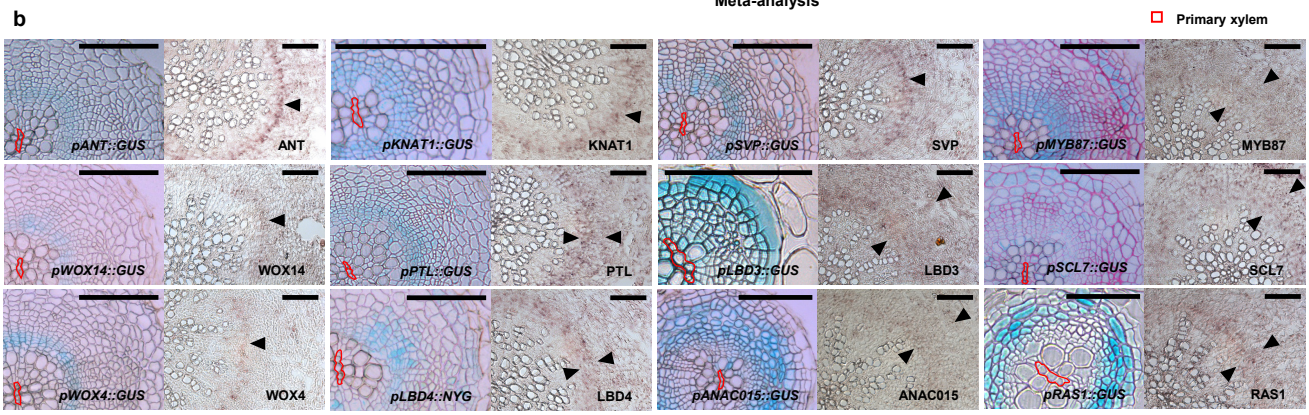
b
Primary xylem
pANT::GUS
ANT
pKNAT1::GUS
KNAT1
pSVP::GUS
SVP
pMYB87::GUS
MYB87
pWOX14::GUS
WOX14
pPTL::GUS
PTL
pLBD3::GUS
LBD3
pSCL7::GUS
SCL7
pWOX4::GUS
WOX4
pLBD4::NYG
LBD4
pANAC015::GUS
ANAC015
pRAS1::GUS
RAS1

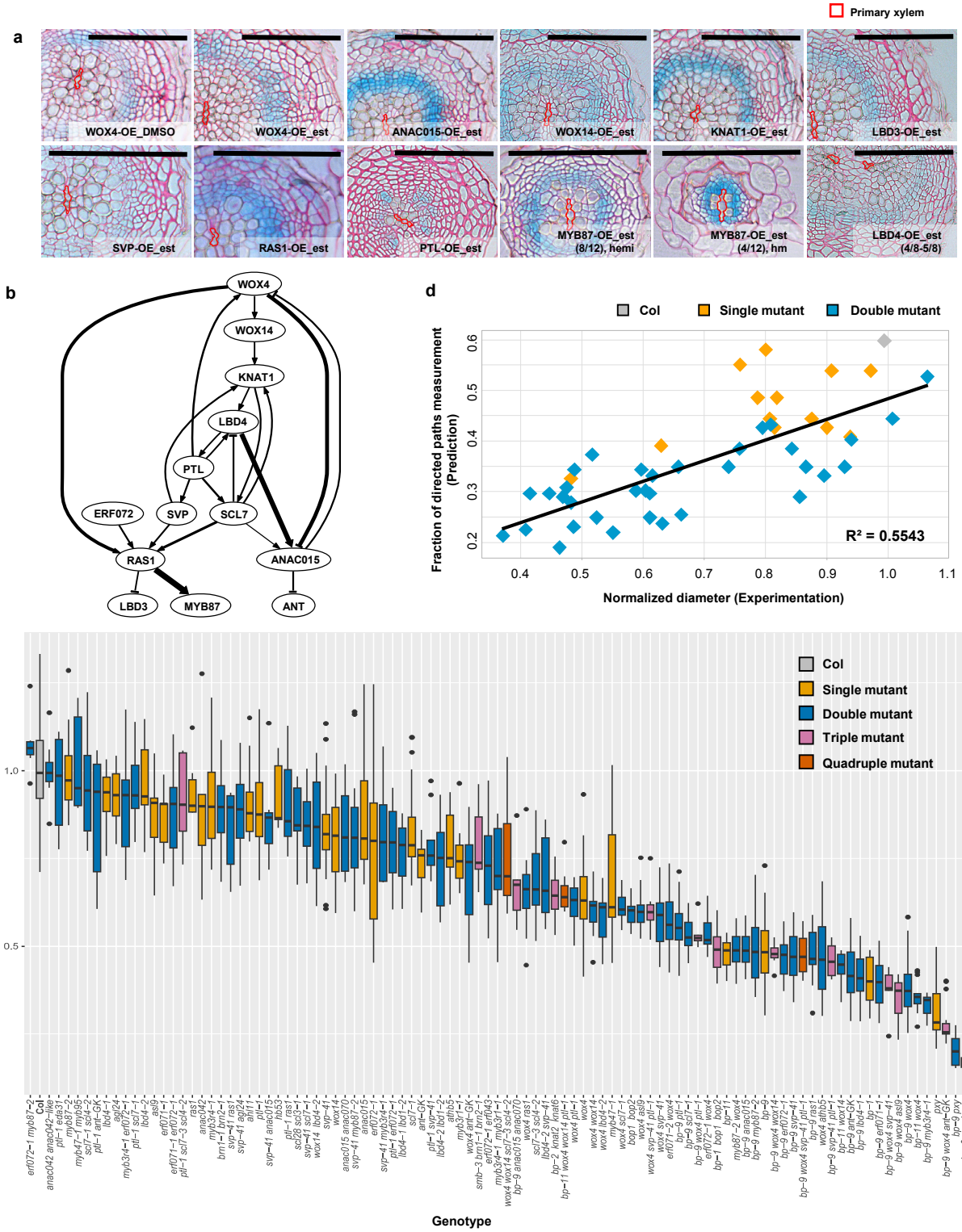
a
Primary xylem
WOX4-OE_DMSO
WOX4-OE_est
ANAC015-OE_est
WOX14-OE_est
KNAT1-OE_est
LBD3-OE_est
SVP-OE_est
RAS1-OE_est
PTL-OE_est
MYB87-OE_est (8/12), hemi
MYB87-OE_est (4/12), hm
LBD4-OE_est (4/8-5/8)
b
WOX4
WOX14
KNAT1
LBD4
PTL
ERF072
SVP
SCL7
RAS1
ANAC015
LBD3
MYB87
ANT
d
Col
Single mutant
Double mutant
Fraction of directed paths measurement (Prediction)
Normalized diameter (Experimentation)
R² = 0.5543
c
Col
Single mutant
Double mutant
Triple mutant
Quadruple mutant
Normalized diameter
Genotype

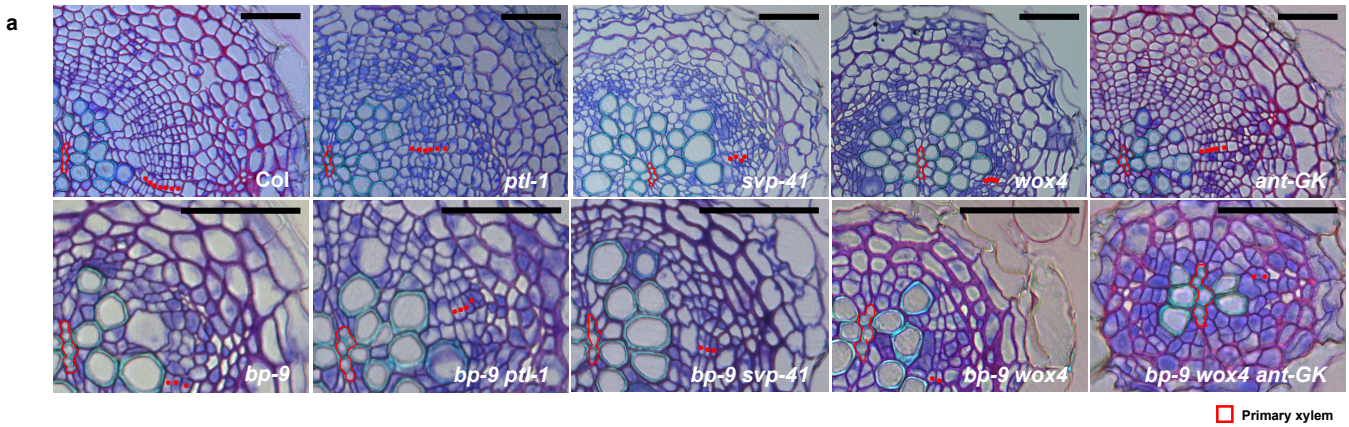
a
Col
ptl-1
svp-41
wox4
ant-GK
bp-9
bp-9 ptl-1
bp-9 svp-41
bp-9 wox4
bp-9 wox4 ant-GK
Primary xylem

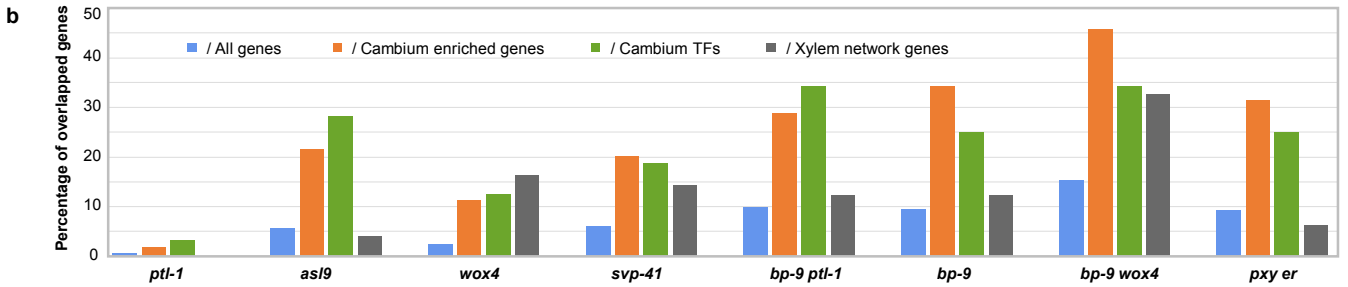
b
Percentage of overlapped genes
50
40
30
20
10
0
/ All genes
/ Cambium enriched genes
/ Cambium TFs
/ Xylem network genes
ptl-1
asl9
wox4
svp-41
bp-9 ptl-1
bp-9
bp-9 wox4
pxy er

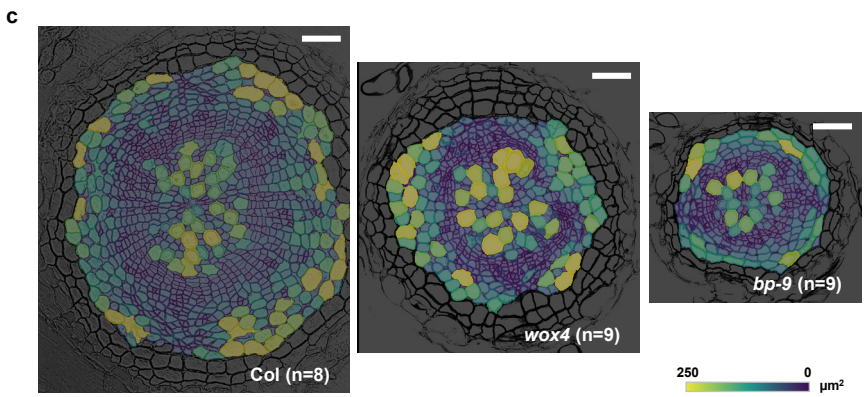
c
Col (n=8)
wox4 (n=9)
bp-9 (n=9)
250
0
µm²

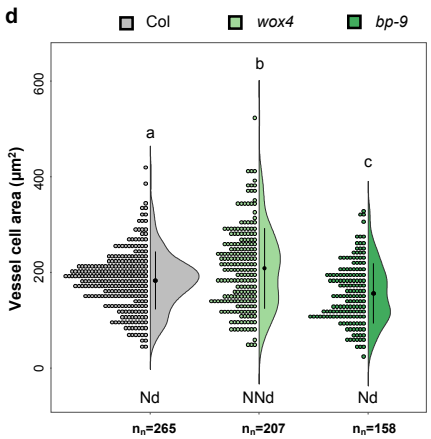
d
Col
wox4
bp-9
Vessel cell area (µm²)
600
400
200
0
a
b
c
Nd
NNd
Nd
n=265
n=207
n=158

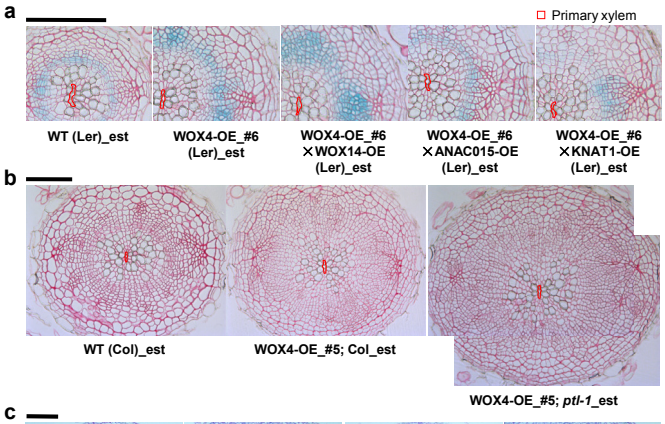
a
Primary xylem
WT (Ler)_est
WOX4-OE_#6 (Ler)_est
WOX4-OE_#6 ×WOX14-OE (Ler)_est
WOX4-OE_#6 ×ANAC015-OE (Ler)_est
WOX4-OE_#6 ×KNAT1-OE (Ler)_est
b
WT (Col)_est
WOX4-OE_#5; Col_est
WOX4-OE_#5; ptl-1_est
c
WOX4-OE_#5; Col _DMSO (n=8)
WOX4-OE_#5; Col _est (n=8)
WOX4-OE_#5; ptl-1 _DMSO (n=8)
WOX4-OE_#5; ptl-1 _est (n=8, 6/8)

Supplementary Information

Supplementary Note

This supplementary note contains additional descriptive and explanatory texts that could not be included in the main text of the manuscript due to space limitations.

1. Meta-analysis identified candidate transcription factors (TFs) on cambium regulation

The expression pattern of *ARR15* was revealed in multiple ways: its expression in procambium (ARRIII domain) was shown previously by *in situ*[42] and in *pARR15::GFP* line (Supplementary Fig. 2a, right bottom); its expression in developing cambium and cambium were displayed in *pARR15::GFP* line (Supplementary Fig. 2a, right). Transcriptome profiling in *pARR15::GFP* positive protoplasts with Fluorescence-activated cell sorting (FACS) was carried out in *Arabidopsis* roots at three stages (ARRI, II and III; Fig 1a; Supplementary Fig. 2a). Since cytokinins are required for radial growth[43,44], parallel profiling was done upon synthetic cytokinin 6-Benzylaminopurine (BAP) treatment (BAP_ARRI, II and III) and data from all six ARR samples were compared with transcriptome of other non-overlapping root cell types to identify the cambium enriched genes (see Methods). Meta-analysis involving multiple steps was performed to identify "cambium TFs". First, two bioinformatics approaches, Differential Expressed Gene (DEG) analysis and gene regulatory Module analysis, were combined to discover the cambium enriched TFs. 34 TFs (Supplementary Table 1c) were identified from 543 cambium enriched genes in the analysis (Supplementary Table 1b), while 174 TFs (Supplementary Table 1e) were taken from the 16 cambium enriched modules (Supplementary Fig.2b; Supplementary Table 1d). 25 TFs that fell into both categories were selected as the initial cambium enriched TFs (Fig. 1a). Second, 12 more genes were added based on their homology to the initial TFs (Supplementary Table 2). Third, although systematic CK inducibility was not investigated in current study, three additional TFs (*ANAC015*,

ANAC042 and *MYB3R4*) that were induced by CK and expressed in ARR samples detected by microarray (Supplementary Table 1b) were also included. *MYR3R1* was added due to its close homology to *MYB3R4*[45]. Altogether 41 genes were included in the list of candidate TFs on cambium regulation (Supplementary Table 2; Fig. 1a).

2. Gene expression atlas of candidate TFs

The radial expression patterns of candidate TFs were investigated with two approaches (Fig.1b; Supplementary Fig. 3): GUS fusion reporter for early stage (1-2 week roots) and RNA *in situ* hybridisation for late stage (5-week roots). If the expression of a candidate gene in cambium region can be detected by at least one approach, it was included as cambium TFs. A subset of cambium TFs were abundantly expressed in cambium, including the previously reported genes *ANT*[16], *WOX4*[12-14], *WOX14*[15] and *KNAT1*[46] (Fig. 1b). Other cambium TFs were expressed in cambium and vascular tissues in roots (Supplementary Table 2; Fig. 1b; Supplementary Fig. 3). *ERF019*, *STY2* and *HB53* were expressed in non-cambium tissues therefore excluded for further studies. IAA3, IAA12 and IAA27 were excluded in the following analysis.

3. Definitions of vascular phenotypes

The vascular phenotypes are defined as follows and illustrated in Supplementary Fig. 1. **a,** The vascular "Diameter" corresponds to the additive measurement of both *radii* from the primary phloem poles to the central primary xylem axis; **b,** The vascular "Cell count" is produced by counting all cells except primary xylem cells that are in contact with the lines used for measuring diameter; **c,** The "Vessel number" corresponds with the total numbers of the differentiated secondary vessels with visible thickened secondary cell wall (expanding vessels are not taken in to account); **d,** The "Xylem area" refers to the size of area within a cycle marking the out boundary of

xylem domain; **e,** The "Cambium area" refers to the size of area between the xylem and cambium boundaries. In GUS stained cambial cell proliferation marker line *pCYCD3,1::GUS* (Ler) plants, "Cambium area" mainly corresponds to the GUS stained area; **f,** The "Vascular area" refers to the whole area of the vasculature; **g,** The classification of different cell types was mainly based on the position and anatomic features (Supplementary Fig. 1d). In addition to "Differentiated vessel", "Other xylem cell", "Cambium cell" and "Phloem cell", "Periderm cell" were also counted. The "Other xylem cell" includes expanding vessels and xylem parenchyma cells while "Periderm cell" includes all cells located outside of the vasculature. The "Total cell number" is the sum of all five cell types as described above.

Extra quantification was carried out to assist the elaboration on the relevant phenotypes. For large scale characterization of mutants (17-day old), the ratio of "Vessel number/Diameter" was calculated to assess the density of vessels (Supplementary Fig. 5c; Supplementary Table 6a, b). For examination of mutants in late stage (7-week old), the ratio of "Xylem area/Vascular area" was calculated to evaluate the proportion of xylem (Supplementary Fig. 8e). In the case of combinatorial overexpression lines (Fig. 4a, b), all cell types were counted in one-quarter of a cross section from independent roots, hence the percentage of certain cell type was obtained by calculating the ratio of "number of certain cell type"/ "total cell number". For selected mutants (Fig.3c, d), the area of each cell was measured using LithoGraphX program (see Methods).

Unless otherwise stated, each measurement were normalized to the average value of the same measurement from wild-type or control plants within the same assay and present as "normalized" or "relative" data, respectively.

4. Inducible overexpression (OE) of cambium TFs caused diverse impacts on cambial activity

The vascular phenotype was examined after 7-day induction for each gene (Fig. 2a; Supplementary Fig. 4). Among all checked lines, WOX4-OE exhibited the strongest effect since the cambium domain (marked by *pCYCD3;1::GUS*; Fig. 2a) was significantly expanded and the overall radial growth (assessed by vascular diameter and vascular area; Supplementary Fig. 4c, d) was increased. WOX14-OE showed similar impact as WOX4-OE but less significant. For ANAC015-OE, although the signal of *pCYCD3;1::GUS* was dramatically enhanced (Fig. 2a; Supplementary Fig. 4b), the overall radial growth was not changed (Supplementary Fig. 4c, d). The influence of KNAT1-OE seemed limited to the xylem domain expansion (Supplementary Fig. 4e). Similarly, overexpressing LBD3-OE could only slightly induced the expansion of the cambium domain (Supplementary Fig. 4b).

In contrast, radial growth was inhibited through the overexpression of *SVP*, *RAS1*, *PTL* and *MYB87* (Fig. 2a; Supplementary Fig. 4). SVP-OE reduced both cambium domain and the overall growth while RAS1-OE only reduced the overall growth but not the cambium domain. Interestingly, PTL-OE strongly inhibited cambial proliferation and xylem differentiation. The inhibitory effect of MYB87-OE appeared to be dose-depended: the phenotypic effect was stronger in homozygous than hemizygous plants (Fig. 2a; Supplementary Fig. 4f; Methods). In the homozygous line of MYB87-OE, although the cambium was maintained as marked by *pCYCD3;1::GUS*, the differentiation of secondary xylem and phloem were almost ceased (Fig. 2a). The effect of LBD4-OE appeared variable since the xylem patterning was affected but only in around half plants (4 out of 8 plants in one transgenic line and 5 out of 8 plants in another transgenic line).

It is noted that in the cases of WOX4-OE and PTL-OE, the root apical growth was inhibited (Supplementary Fig. 4f). Such apical growth phenotypes were not further disturbed when WOX4-OE was combined with other OE lines (Supplementary Fig. 12d) or mutant background (*ptl-1*; Supplementary Fig. 13d). Further anatomic analysis of the root tip of WOX4-OE revealed that the swelling of root tip, which is reported previously in the constitutively overexpressed WOX4 line[13],

was associated with massive cell proliferation predominately in the ground tissues (Supplementary Fig. 4g).

5. Cambium transcriptional regulatory network construction

13 TFs that met the criteria as following were selected for the cambium transcriptional network construction: (1) sufficient to affect cambial activity when overexpressed (*WOX4*, *ANAC015*, *WOX14*, *KNAT1*, *LBD3*, *RAS1*, *SVP*, *PTL*, *MYB87* and *LBD4*; Fig 2a), or (2) representative of other cambium expressed TF families (*ANT* [AP2-like family], *ERF072* [ERF family] and *SCL7* [GRAS family]; Supplementary Table 2).

For construction of the network, if the overexpression of gene A produced a statistically significant increase (or decrease) in expression of gene B, the network would contain a directed activatory (or inhibitory) connection from gene A to gene B. The network derived in this way had a number of feed-forward loops. This is because an overexpressed gene is likely to affect the expression not only of those genes it has a direct regulatory relationship with, but also those genes that are further downstream. Hence if overexpression of gene A leads to an increase in the expression of gene B, and increased expression of gene B leads to increased expression of gene C, then gene A will also appear to be connected to gene C, creating a feed-forward loop. In an attempt to remove redundant connections of this kind, we created a pared-back version of the network (See Methods) and present such simplified version as our final network (Fig. 2b).

6. Characterization of vascular phenotypes in mutants

The parameters used to illustrate vascular phenotypes are described as above. Quantification of mutant phenotypes was present in Supplementary Table 6a and b. Mutants showing significant changes on general radial growth (based on Diameter) or cambial cell proliferation (based on Cell

count) compared with Col were indicated with orange squares while mutants displaying increased or decrease xylem vessel density (based on the ratio of Vessel number/Diameter) compared with Col were indicated with blue squares. Mutants with phenotypes on both categories were indicated with two-colour squares divided diagonally.

Collectively, among the analysed 98 alleles (representing 91 genotypes) of mutants (Fig. 2c; Supplementary Fig. 5a-c (left)), except *pxy*, *bp-9 pxy* and *bp-9 wox4 pxy*, all the other 95 alleles involved the mutations of 27 cambium TFs (Supplementary Table 6a). Two alleles were examined for five genotypes (*bp wox4*, *lbd4*, *lbd4 lbd1*, *scl7 scl4* and *anac015 anc070* (also known as *brn1-1 brn2-1*)) while three alleles were checked for *KNAT1* mutant *bp* (*bp-1*, *bp-9* and *bp-11*). Our investigation found that 73 alleles (representing 69 genotypes) of TF mutants displayed cambial activity (marked as yellow in Supplementary Table 6a) defect compared with Col. Since 7 TF genotypes, *ant*[16], *wox4*[13-15], *wox14*[15], *wox4 wox14*[15], *bp*[46,47], *bop1 bop2*[47] and *bp bop1 bop2*[47] were reported previously in the context of radial growth, our study therefore identified 62 novel TF genotypes that demonstrated the cambium defect. The observation that vessel density was increased compared with Col in a number of mutants (Supplementary Fig. 5c and Supplementary Table 6a) implied the potential roles of corresponding TFs during xylem differentiation.

In all analysed mutants, no obvious defect of root apical growth was observed except for *smb-3 brn1-1 brn2-1*, in which root length was significantly reduced (data not shown), suggesting the studied TFs were more specific to radial growth.

6.1 Examination of single mutant phenotypes

We first investigated all available single mutants for the candidate TFs on cambium regulation. Overall radial growth (Fig. 2c) and cambium cell proliferation (Supplementary Fig. 5a) in a number of mutants including *bp* (with three alleles), *wox4*, *svp*, *ant* and *asl9* was significantly decreased

(Supplementary Table 6a, b). In addition, analysis of "Vessel number/Diameter" uncovered that regardless of the reduced radial growth (Fig. 3a) in *svp*, the density of the differentiated xylem vessel was increased (Supplementary Fig. 5c; Supplementary Table 6a, b) and this xylem phenotype was further strengthened during fibre formation stage (Supplementary Figs. 1a and 8d,e).

6.2 Characterization of combinatorial mutants within the same family revealed the functional interactions

Among the 95 loss-of-function TF mutant alleles we characterized, more than half genotypes were on the predicted mutant list (Supplementary Table 3c). Additionally, genotypes beyond the network, involving homologous TFs and higher order mutants to the 13 TFs, were also included for analysis.

We checked the double or triple mutants within each TF family to explore genetic interactions in this TF family. We first checked the previously reported mutant *wox4 wox14* and found that *wox14* only enhanced *wox4* phenotype significantly in fibre formation stage (Supplementary Table 6a,d; Supplementary Fig. 8d, e) as reported in hypocotyl[15]. For MADS family, *SVP* was epistatic to its close homologue *AGL24* since double mutant displayed the same xylem phenotypes as *svp* (Supplementary Fig. 6c), confirming their interaction found in regulating flowering time[48]. Although *bp* alone already revealed strong defect in cambial activity, this defect was not enforced with the mutations of its homologs *KNAT2* and *KNAT6*. On the contrary, *KNAT2* and *KNAT6* seemed acting antagonistically to *KNAT1* as *knat2 knat6* partially rescued *bp* vascular phenotypes (Supplementary Fig. 6c; Supplementary Table 6), as the similar interaction observed in the inflorescence development[49]. Since two TFs *BLADE ON PETIOLE 1* (*BOP1*) and *BOP2* were known as downstream targets of *KNAT1*, we also checked the phenotype of *bp-1 bop1 bop2*. We found although *bop1 bop2* had decreased growth, it can partially suppressed *bp-1* phenotype

regarding to cambial activity (Supplementary Fig.6c; Supplementary Table 6), confirming their interaction during fibre formation as reported earlier[47].

Among all TF families we examined, functional redundancy was found in a few families but in different manners. For Trihelix family, xylem vessel density was enhanced when both *PTL* and its homolog *EMBRYO SAC DEVELOPMENT ARREST 31* (*EDA31*) were mutated (Supplementary Fig. 6a; Supplementary Table 6b). Although no significant phenotype was observed in single mutant, the radial growth was reduced when two members from GRAS (SCLs), LBD or ERF family were knocked out (Supplementary Fig.6a; Supplementary Table 6b). Within R1R2R3-MYB family, each single mutant exhibited mild defect on radial growth and additive effect was observed in the double mutant (Supplementary Fig. 6b; Supplementary Table 6b). These data altogether indicated that diverse interactions existed among homologous genes.

6.3 Phenotypic analyses of combinatorial mutants revealed the functional redundancy between various TF families

We further evaluated the function redundancy between different TF families by making a list of crosses among mutants from various TF families. We analysed several *wox4* double mutants containing but only *athb5* (Supplementary Fig. 7a) could significantly enhance *wox4* defect in addition to *bp* (Fig. 3a). Although *ptl* can partially suppress *bp* phenotype (Fig. 3a), it did not affect *wox4* in the same way (Supplementary Fig. 7a). Interestingly, although the density of xylem vessels was increased in the single mutant of *svp-41*, *ptl-1*, *lbd4-2* and *wox4* (Supplementary Table 6a; Supplementary Fig. 5c), the phenotype was only enfored in *ptl-1 svp-41* and *lbd4-2 svp-41*, in which vessel differentiation was markedly promoted, indicating their roles in regulating vessel formation synergistically (Supplementary Fig. 7a; Supplementary Fig. 5c). Combination of *bp-9* and *svp-41* led to the increase of vessel density in early stage (Fig. 3a and Supplementary Table 6a), however, this effect was less strong in late stage as an intermediate phenotype on xylem fibre

formation was shown (Supplementary Fig. 8d, e). Taken together, it seemed that *SVP* is epistatic to other TFs in most cases concerning the regulation of xylem development. Similarly, *lbd4* mutation did not strengthen the cambial activity defect but cause xylem vessel phenotype of *bp* (Supplementary Fig. 7b). Analyses of higher order mutants containing *bp*, *wox4*, *ptl* and *svp* further confirmed that *ptl* suppressed *bp* phenotype (Supplementary Fig. 9a; Supplementary Table 6a). The finding that *ant* could not affect significantly the single mutant of either *wox4* or *bp-9* but only in *bp-9 wox4* (Supplementary Table 6a, b) implied more complicated genetic interactions among them. Our phenotypic analyses of combinatorial mutants suggested the involved cambium TF families regulate cambial activity redundantly.

Supplementary Information References

42. Mahonen, A.P. et al. Cytokinin signaling and its inhibitor AHP6 regulate cell fate during vascular development. *Science* **311**, 94-98 (2006).
43. Matsumoto-Kitano, M. et al. Cytokinins are central regulators of cambial activity. *Proceedings of the National Academy of Sciences of the United States of America* **105**, 20027-20031 (2008).
44. Nieminen, K. et al. Cytokinin signaling regulates cambial development in poplar. *Proceedings of the National Academy of Sciences of the United States of America* **105**, 20032-20037 (2008).
45. Haga, N. et al. R1R2R3-Myb proteins positively regulate cytokinesis through activation of KNOLLE transcription in Arabidopsis thaliana. *Development* **134**, 1101-1110 (2007).
46. Liebsch, D. et al. Class I KNOX transcription factors promote differentiation of cambial derivatives into xylem fibers in the Arabidopsis hypocotyl. *Development* **141**, 4311-4319 (2014).
47. Woerlen, N. et al. Repression of BLADE-ON-PETIOLE genes by KNOX homeodomain protein BREVIPEDICELLUS is essential for differentiation of secondary xylem in Arabidopsis root. *Planta* **245**, 1079-1090 (2017).
48. Gregis, V., Sessa, A., Colombo, L. & Kater, M.M. AGL24, SHORT VEGETATIVE PHASE, and APETALA1 redundantly control AGAMOUS during early stages of flower development in Arabidopsis. *Plant Cell* **18**, 1373-1382 (2006).
49. Ragni, L., Belles-Boix, E., Gunl, M. & Pautot, V. Interaction of KNAT6 and KNAT2 with BREVIPEDICELLUS and PENNYWISE in Arabidopsis inflorescences. *Plant Cell* **20**, 888-900 (2008).

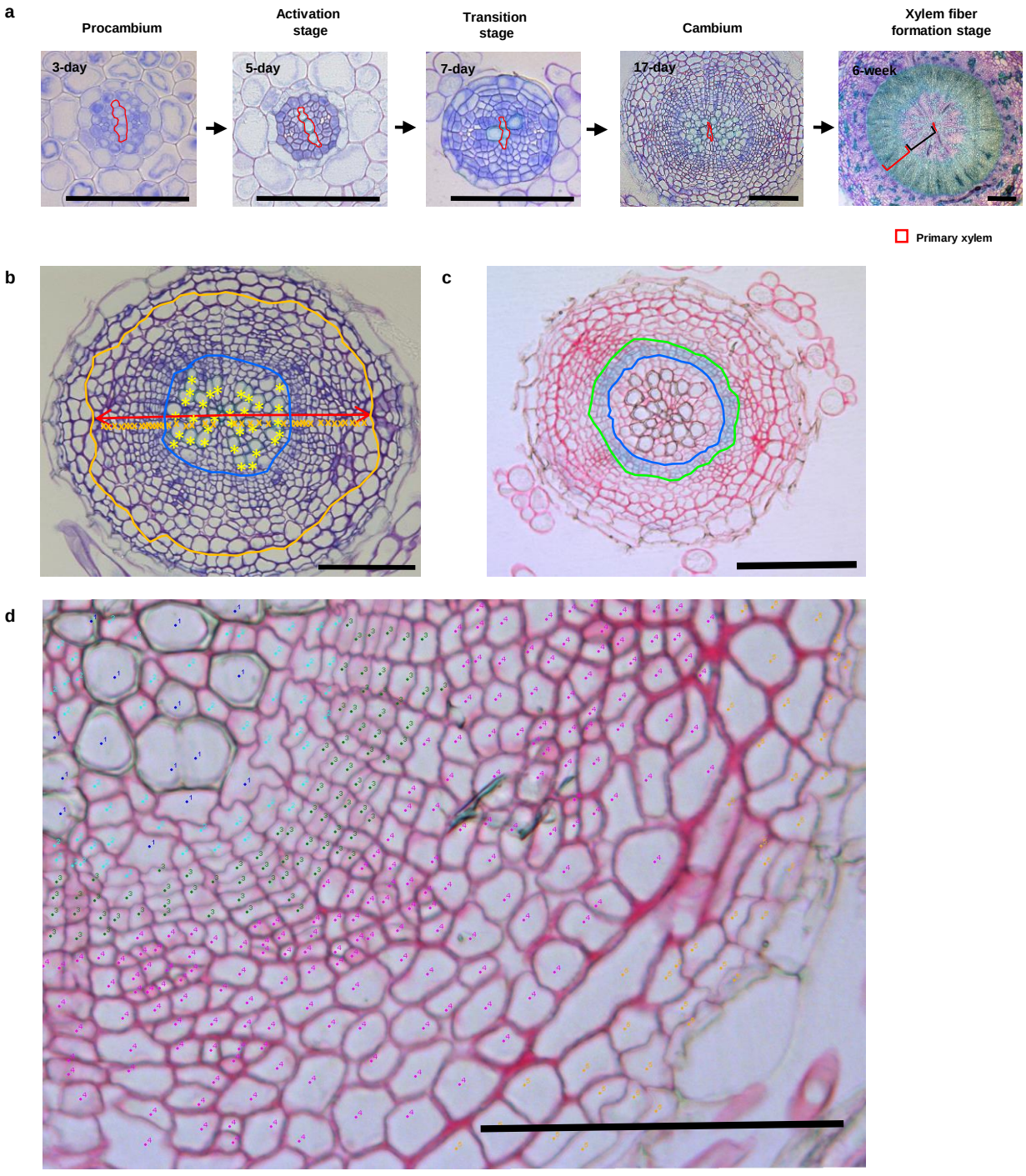

Supplementary Fig. 1 | The dynamic development of vascular cambium and quantification of vascular phenotypes in *Arabidopsis* roots.

a, Toluidine blue O-stained cross sections from roots of wild-type (Col) sampled at various temporal stages (3-day, 5-day, 17-day, 6-week) growing under long-day condition. Sections were

taken at 5mm below the hypocotyl-root junction. The procambial cells start periclinal cell division in the activation stage (5-day) and produce secondary xylem cells in the transition stage (7-day) and full cylinder of cambium could be found in cambium stage (17-day) with additional xylem fibre formation occurred much later (6-week). Black square indicated the xylem vessel differentiation stage and red bracket indicated the xylem fibre formation stage on 6-week cross section. The primary xylem axis is indicated in all stages. **b-d,** Illustration of measurements on root cross sections. **b,** Red lines with arrow indicate vascular "Diameter". All cells marked with orange "x" were counted to produce vascular "Cell count". Differentiated vessels marked with yellow "*"were counted to generate "Vessel number". The inner blue cycle was marked as the boundary of xylem domain and the outer orange cycle was marked as the boundary of the whole vasculature. The area within the blue cycle was measured as "Xylem area" while the area within the orange cycle was measured as "Vascular area". **c,** A cross section of GUS stained followed by Ruthenium red contrast stained roots in a cambial cell proliferation marker line *pCYCD3,1::GUS* (Ler). The area with GUS staining between the inner blue cycle and outer green cycle was measured as "Cambium area". **d,** Five cell types (1-5) were marked with different colours and counted with Fiji (1.0)/ImageJ (1.47v) in one quarter of a root cross section. "1" marks "Differentiated vessel", "2" marks "Other xylem cell", "3" marks "Cambium cell", "4" marks "Phloem cell", "5" marks "Periderm cell". Scale bars, 100µm. All experiments were repeated at least three times.

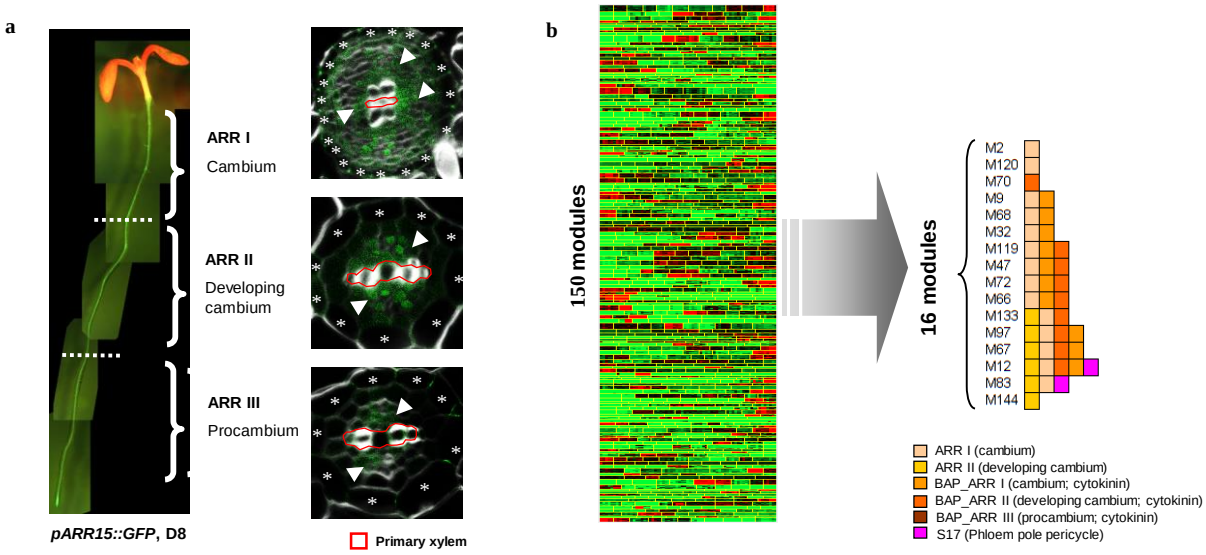

Supplementary Fig. 2 | Using *ARR15* as a cambium marker to identify cambium enriched genes and gene modules.

a, Confocal microscopic images of a *pARR15::GFP* seedling (left) and 200-µm thick vibratome cross sections taken at three positions (ARRI, ARRII and ARRIII) of a 8-day old *Arabidopsis* root (right). Cell wall was stained with calcofluor-white. The expression of *ARR15* is restricted in procambium (ARRIII) with weak expression but the expression seemed broad in ARRI domain since the expression in pericycle was also observed. Endodermal cells were marked with white "*"; *pARR15::GFP* signals were indicated with white arrow-heads. The primary xylem axis is marked in red. **b,** 16 Cambium enriched modules were identified out of 150 gene modules.

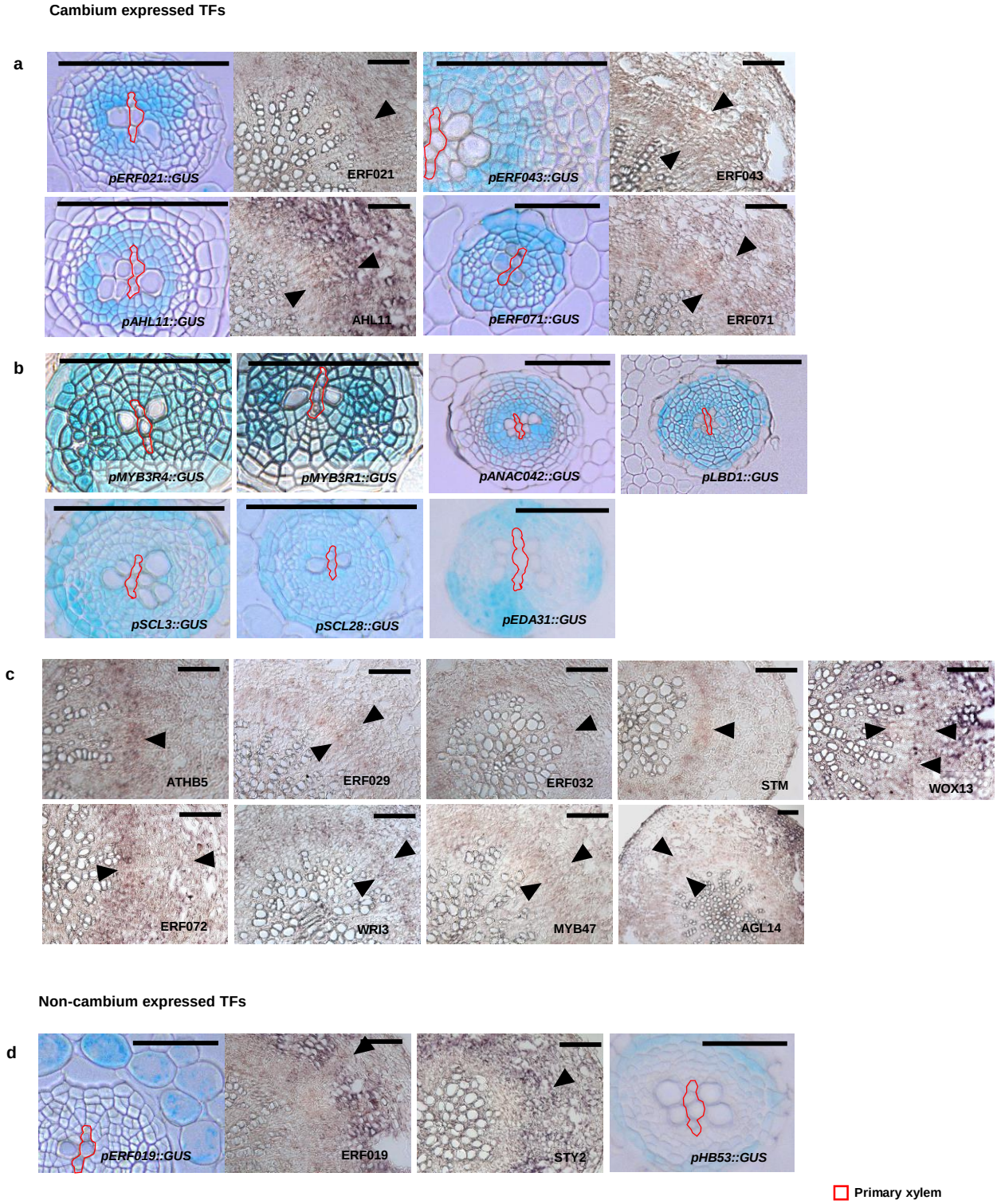

Supplementary Fig. 3 | Expression atlas of candidate transcription factors (TFs) on cambium regulation during radial growth in *Arabidopsis* roots.

a-c, Radial expression patterns of cambium expressed TFs**. a,** Radial expression pattern was

checked by both transcriptional GUS reporter line in 1-2 week old roots and RNA *in situ* hybridisation in 5-week old roots. **b**, Radial expression pattern was checked only by transcriptional GUS reporter line in 1-2 week old roots. **c**, Radial expression pattern was checked only by RNA *in situ* hybridisation in 5-week old roots. **d**, Radial expression pattern of non-cambium expressed TFs detected by transcriptional GUS reporter line in 1-2 week old roots and/or RNA *in situ* hybridisation in 5-week old roots. All GUS staining was repeated at least twice with similar results. For *in situ* hybridisation, at least 10 Col plants were examined for each gene with similar patterns. The primary xylem axis is marked on the GUS sections. Black arrow-heads indicate the *in situ* signals. Scale bars, 100μm.

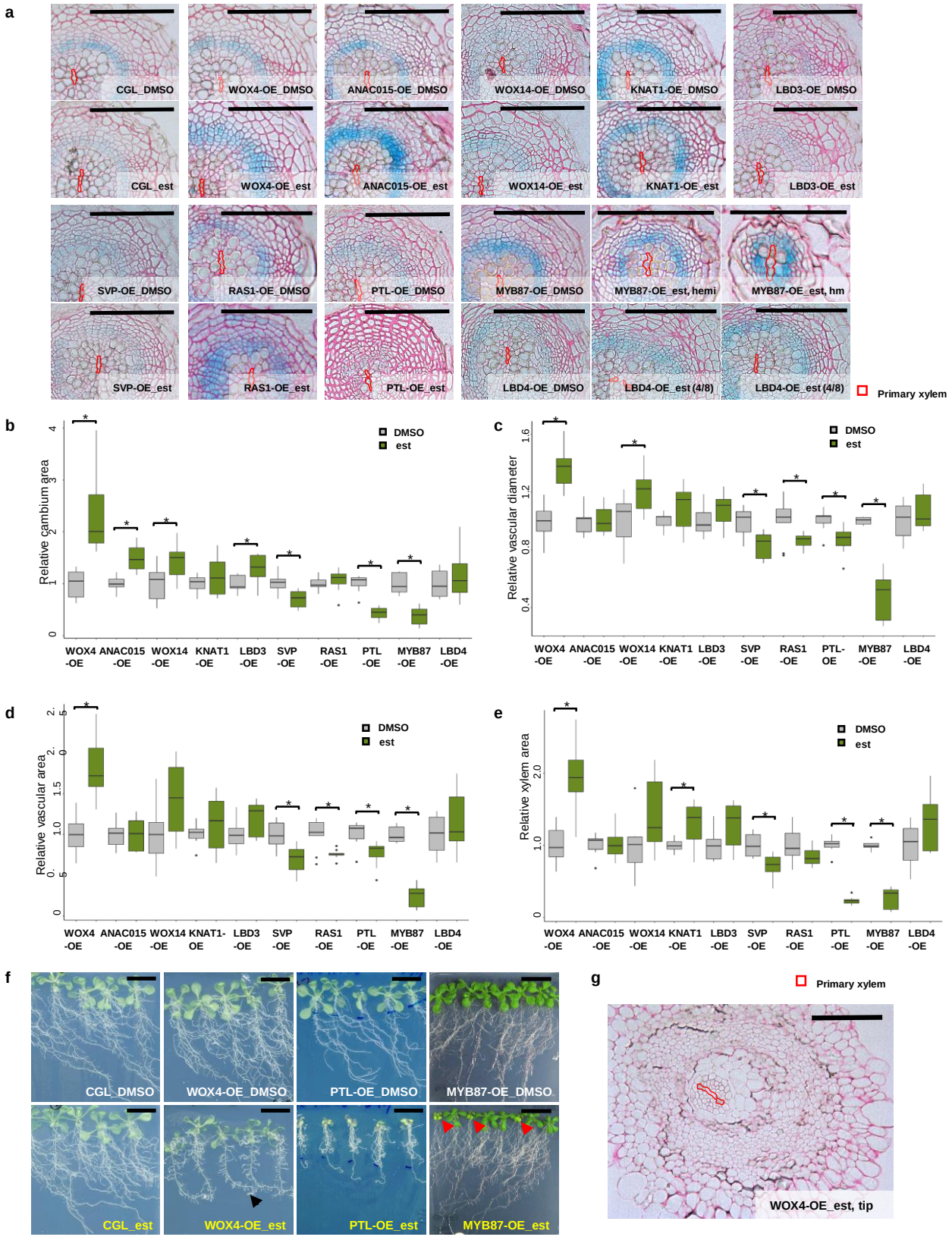

Supplementary Fig. 4 | Characterization of vascular phenotypes in overexpression (OE) lines.

a, Inducible overexpression (OE) lines of cambium transcription factors (TFs) that affected cambial activity. Anatomical phenotype of a second replicate was shown for all OE lines presented in **Fig. 2a.** All lines were generated in a cambial cell proliferation marker line *pCYCD3,1::GUS* (Ler) (referred to as CGL). Cross sections of GUS stained followed by Ruthenium red contrast stained roots of control (DMSO) and 5µM estradiol (est) treated plants from each OE line and CGL. Each gene was induced for 7 days in 7-day old seedlings. For MYB87-OE, segregation of phenotype was observed, "hemi" refers to hemizygous plants; "hm" refers to homozygous plants. **b-e,** Vascular phenotypes including cambium area, marked by *pCYCD3;1::GUS* (**b**), vascular diameter **(c),** vascular area **(d)** and xylem area **(e)** were quantified in both control DMSO and est treated plants and the obtained data were normalized to the DMSO for each OE line presented in **Fig. 2a**. Box-and-whisker plots are centred at the median, which splits first and third quartiles. Whiskers show range and black dots represent outliers. **P*<0.05 (two-tailed Student's t-test); exact n (number of independent roots) and *P* value for the analysis can be found in **Supplementary Table 5a**. **f**, The plate images of 14-day old plants treated for 7-days on DMSO (upper) or est (lower) plates for wild-type (CGL) and several OE lines. Note the root tip phenotypes in WOX4-OE_est and PTL-OE_est plates. Black arrow indicated the enlarged root tip on WOX4-OE_est plate. Red arrowheads indicated the homozygous plants on MYB87-OE_est plate. **g**, Ruthenium red-stained cross section of an enlarged root tip from WOX4-OE_est plate. The primary xylem axis is marked in red in **a** and **g**. All experiments were repeated at least three times. Scale bars, 2cm in **f** and 100µm in **a** and **g**.

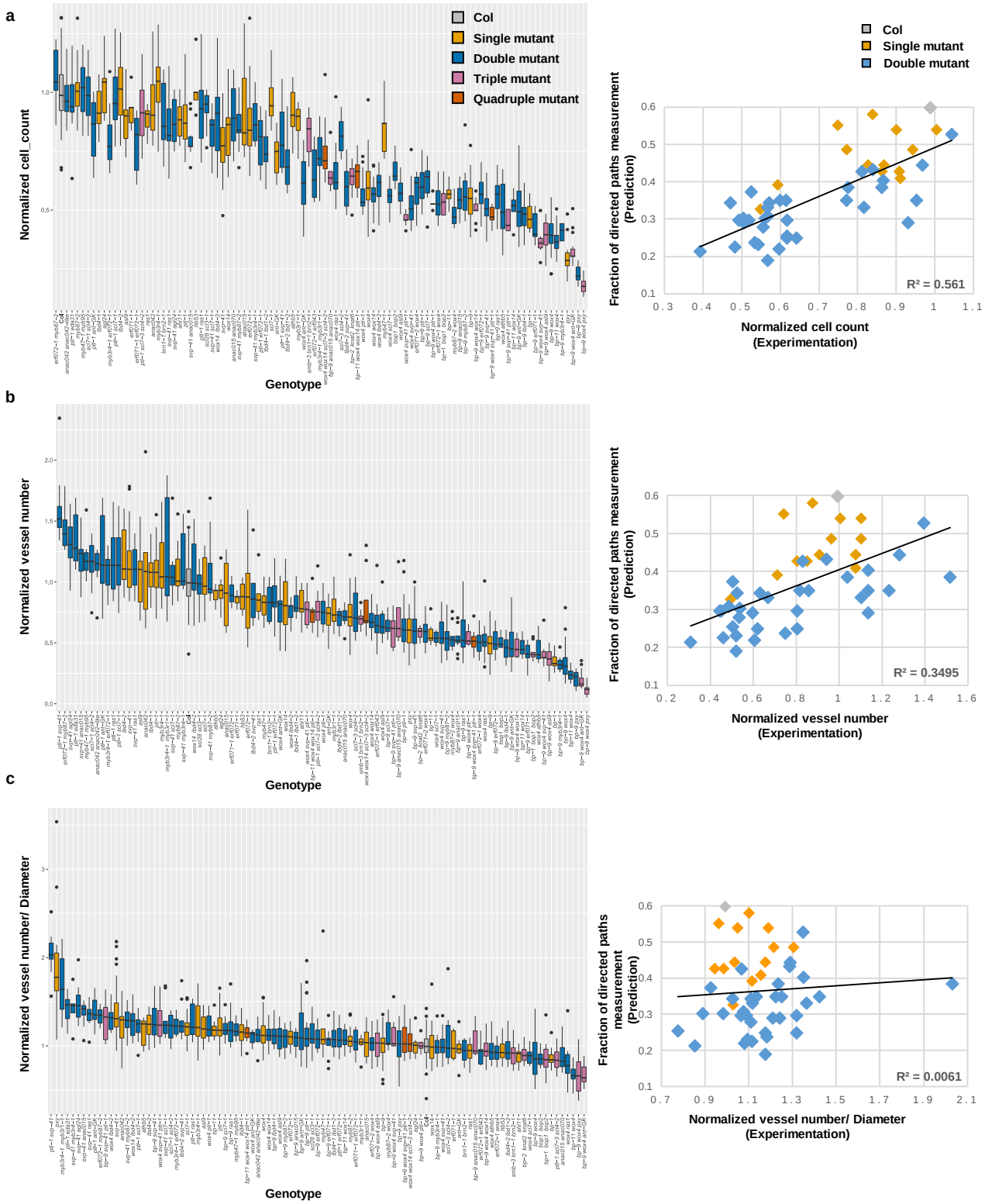

Supplementary Fig. 5 | characterization of vascular mutants and comparison with predicted phenotype severity.

a, The normalized "cell count" was displayed among 17-day old wild-type (Col) and mutants (left

panel); the correlation between the predicted phenotype severities indicated as “Fraction of directed paths measurement” and the normalized cell count (right panel). The genotypes were ordered as the same as present in **Figure 2c**. **b**, The normalized “vessel number” was displayed among 17-day old Col and mutants (left panel); the correlation between the predicted phenotype severities indicated as “Fraction of directed paths measurement” and the normalized vessel number (right panel). **c**, The normalized ratio of “Vessel number/Diameter” was displayed among 17-day old Col and mutants (left panel); the correlation between the predicted phenotype severities indicated as “Fraction of directed paths measurement” and the ratio of “Vessel number /Diameter” (right panel). Data were collected from a number of independent experiments and phenotype data for each mutant were normalized to the Col within the same analysis. Box-and-whisker plots are centred at the median, which splits first and third quartiles. Whiskers show range and black dots represent outliers. Linear regression model was adopted and R-squared (R^2) was used to measure the correlation. The genotypes used in the analysis was listed in **Supplementary Dataset 1**. For each genotype, the median of phenotype, the frequency of significance (examined by a two-tailed Student’s t-test in each experiment) of the phenotype observed in multiple experiments and exact total number of independent roots (N) were listed in **Supplementary Table 6a**.

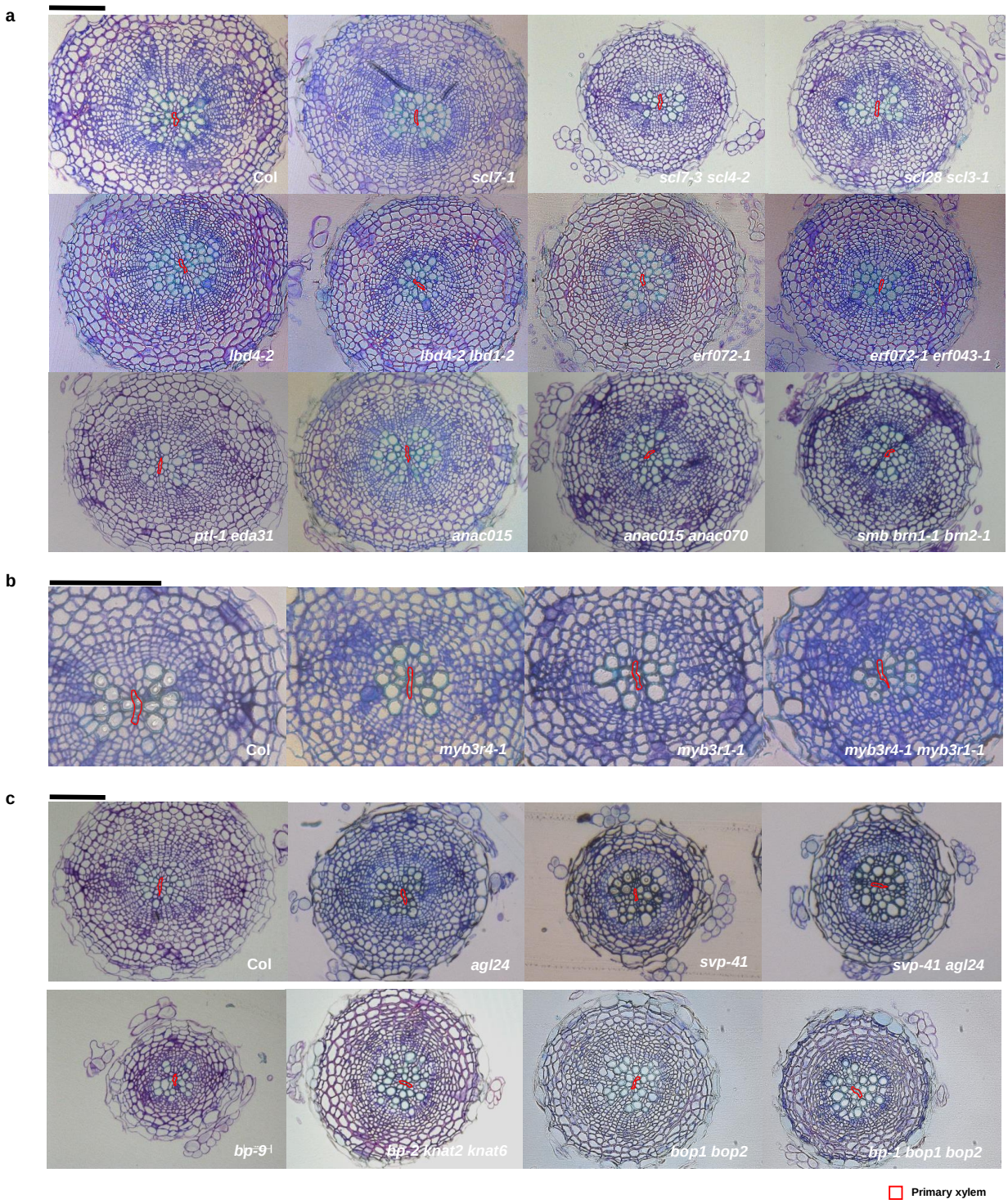

Supplementary Fig. 6 | Genetic interaction within the same transcription factor (TF) family on regulation of cambial activity.

a, Vascular phenotypes were enhanced in various manners when two TFs within the same family in GRAS (SCLs), LBD, ERF and Trihelix (*PTL* and *EDA31*) were simultaneously mutated. No

significant additive effects were observed in NAC families. **b,** Vascular phenotypes were enhanced in the double mutants of two homologous R1R2R3-MYB genes, *MYB3R1* and *MYB3R4*. **c,** Investigation on genetic interaction in MADS-box family and type I KNOX family. Mutations of *SVP* and its close homologue gene *AGL24* resulted in the similar phenotype on xylem vessel differentiation. Mutations of *KNAT2* and *KNAT6* (the two homologous genes of *KNAT1*) partially suppressed cambial activity defect of *bp*. Mutations of *BOP1* and *BOP2* (the known target genes of *KNAT1*) also partially rescued *bp* radial growth phenotypes. Cross sections were taken from the main roots 5mm below hypocotyl-root junction of 17-day old seedlings and stained with Toluidine blue O. All measurements of vascular phenotypes and statistical analysis for all genotypes can be found in **Supplementary Table 6a, b**. The primary xylem axis is marked in red. For each genotype, the exact number of independent experiments and the number of roots in each experiment was listed in **Supplementary Table 6a**. Scale bars, 100μm.

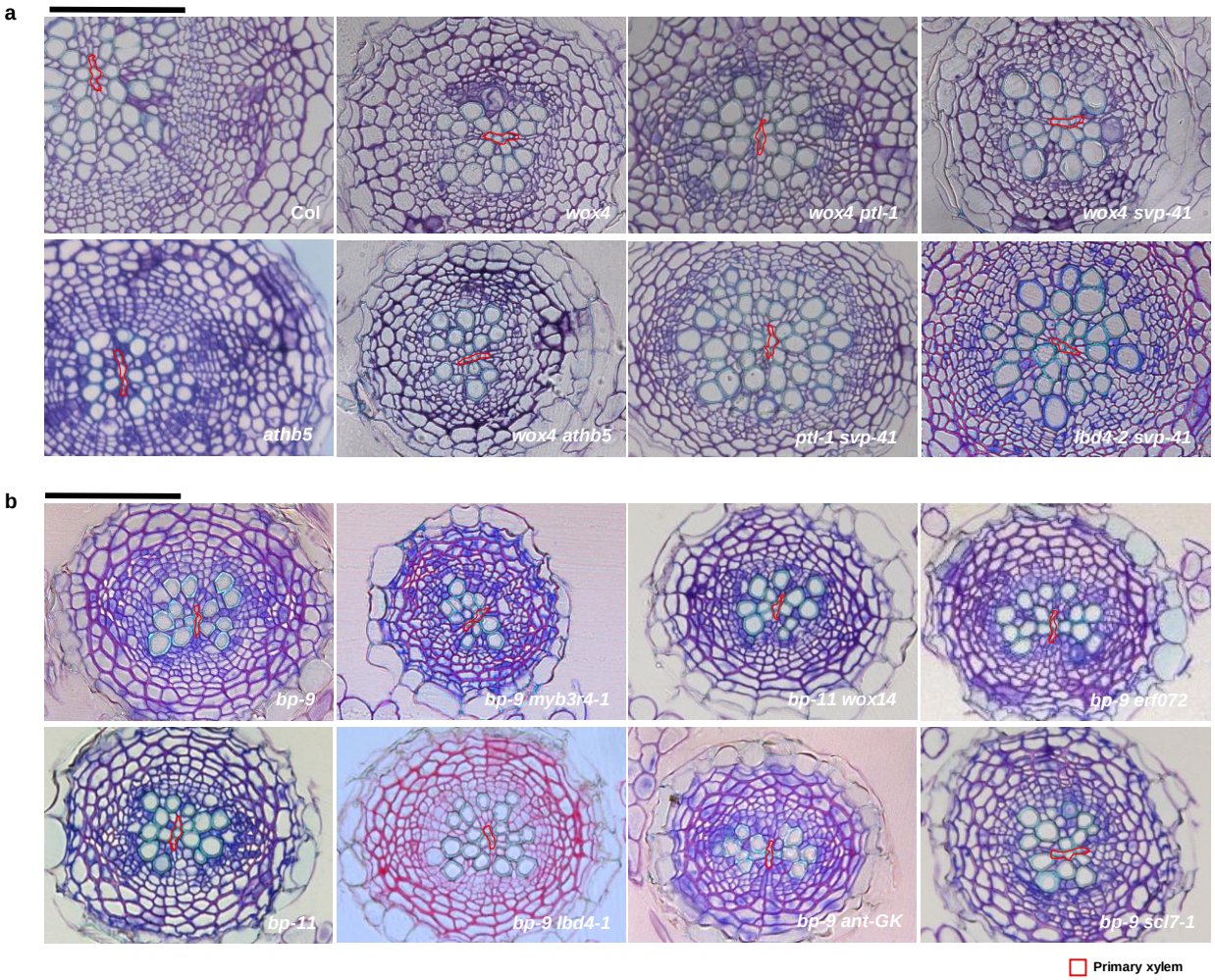

Supplementary Fig. 7 | Genetic interaction between various transcription factor (TF) families on regulation of cambial activity.

a, Anatomic phenotypes characterization in double mutants indicated function redundancy between different TF families. *athb5* and *svp* mutation could enhance the cell proliferation and xylem phenotype of *wox4*, respectively, whereas *ptl* mutation could not significantly affect *wox4* phenotypes. Double mutant of *ptl* and *svp* resulted in largely increase of xylem vessel numbers. Double mutant of *lbd4* and *svp* led to vascular defects in both cambial cell proliferation and xylem vessel differentiation. **b,** Anatomic phenotypes characterization of *bp* combinatorial mutants. *myb3r4*, *wox14* and *erf072* mutation could enforce the cambial cell proliferation defect of *bp* whereas *svp* and *lbd4* mutation elevated the vessel differentiation of *bp*. On the other hand, *ant* and

scl7 mutation could not affect *bp* phenotypes. Cross sections were taken from the main roots 5mm below hypocotyl-root junction of 17-day old seedlings and stained with Toluidine blue O with the exception of *bp-9 lbd4-1* which was stained with Ruthenium Red. All measurements of vascular phenotypes and statistical analysis for all genotypes can be found in **Supplementary Table 6**. The primary xylem axis is marked in red. For each genotype, the exact number of independent experiments and the number of roots in each experiment was listed in **Supplementary Table 6a**. Scale bars, 100μm.

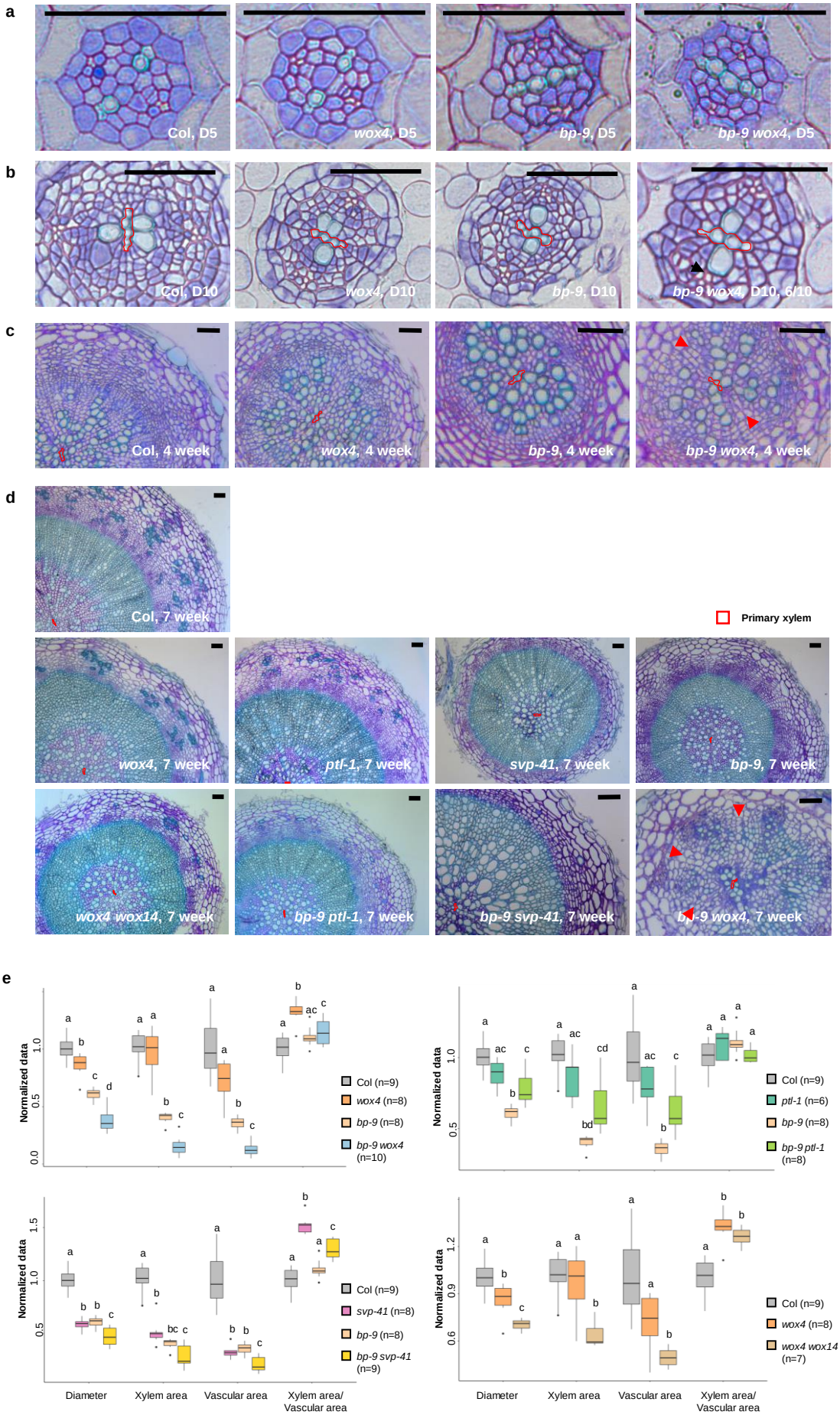
a
Col, D5
wox4, D5
bp-9, D5
bp-9 wox4, D5
b
Col, D10
wox4, D10
bp-9, D10
bp-9 wox4, D10, 6/10
c
Col, 4 week
wox4, 4 week
bp-9, 4 week
bp-9 wox4, 4 week
d
Col, 7 week
Primary xylem
wox4, 7 week
ptl-1, 7 week
svp-41, 7 week
bp-9, 7 week
wox4 wox14, 7 week
bp-9 ptl-1, 7 week
bp-9 svp-41, 7 week
bp-9 wox4, 7 week
e
Normalized data
Col (n=9)
wox4 (n=8)
bp-9 (n=8)
bp-9 wox4 (n=10)
ptl-1 (n=6)
bp-9 ptl-1 (n=8)
svp-41 (n=8)
bp-9 svp-41 (n=9)
wox4 wox14 (n=7)
Diameter
Xylem area
Vascular area
Xylem area/ Vascular area

Supplementary Fig. 8 | Temporal progression of mutant phenotypes.

a, Root anatomic phenotypes of wild-type (Col), *wox4*, *bp-9* and *bp-9 wox4* were checked at cambium initiation stage (5-day, D5), no cell division defect was observed. **b,** Root anatomic phenotypes of Col, *wox4*, *bp-9* and *bp-9 wox4* were checked at transition stage (10-day, D10), the frequency of "xylem adjacent to phloem" phenotype indicated by black arrowhead in *bp-9 wox4* was observed in *bp-9 wox4* (6/10), *bp-9* (2/10), *wox4* (1/10) and Col (0/10). **c,** Root anatomic phenotypes of Col, *wox4*, *bp-9* and *bp-9 wox4* were checked at 4-week, delayed vessel differentiation along primary xylem axis was observed in *bp-9 wox4* as indicated by red arrowheads. **d,** Root anatomic phenotypes of Col, single and double mutants of major cambium regulators were checked at fibre formation stage (7-week). Significant abortion of cambial activity leading to the gaps of vasculature was observed in *bp-9 wox4*, as indicated by red arrowheads. All sections were taken from the main roots 5mm below stem-hypocotyl junction of plants at different ages and stained with toluidine blue O. The primary xylem axis is marked in **b**-**d**. Scale bars, 50μm. All experiments were repeated at least twice in **a-d**. **e,** Quantification on vascular phenotypes in 7-week old Col and mutants presented in **d**. For all genotypes, vascular "Diameter", "Xylem area", "Vascular area" were measured and normalized to Col. The ratio between xylem area against vascular area was calculated. Box-and-whisker plots are centred at the median, which splits first and third quartiles. Whiskers show range and black dots represent outliers. Different letters indicate a significant difference (P<0.05) based on a one-way ANOVA (the exact P value for each comparison can be found in **Supplementary Dataset 2b**). n, independent roots.

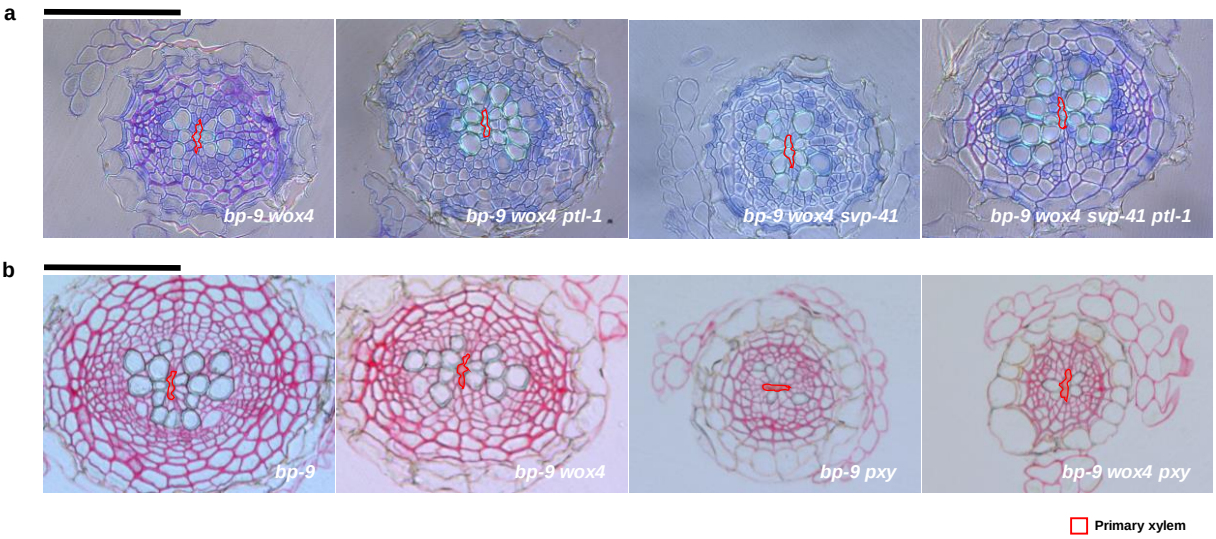

Supplementary Fig. 9 | Synergistic effects of KNOX and other pathways in regulating cambial activity and radial growth.

a, Anatomic phenotypes of higher order combinatorial mutants among *bp*, *wox4*, *svp* and *ptl* indicated the interactions among them. All experiments were repeated at least twice. **b,** Cambial activity was largely disrupted in *bp-9 pxy* and *bp-9 wox4 pxy*, suggesting the synergistic effects of KNAT1 pathway and PXY-WOX4 pathway in regulating cambial activity. All experiments were repeated three times. Sections were taken from the main roots 5mm below hypocotyl-root junction of 17-day old seedlings and cross sections were stained with Toluidine blue O **(a)** or Ruthenium Red **(b)**. The primary xylem axis is marked in all lines. Scale bars, 100μm.

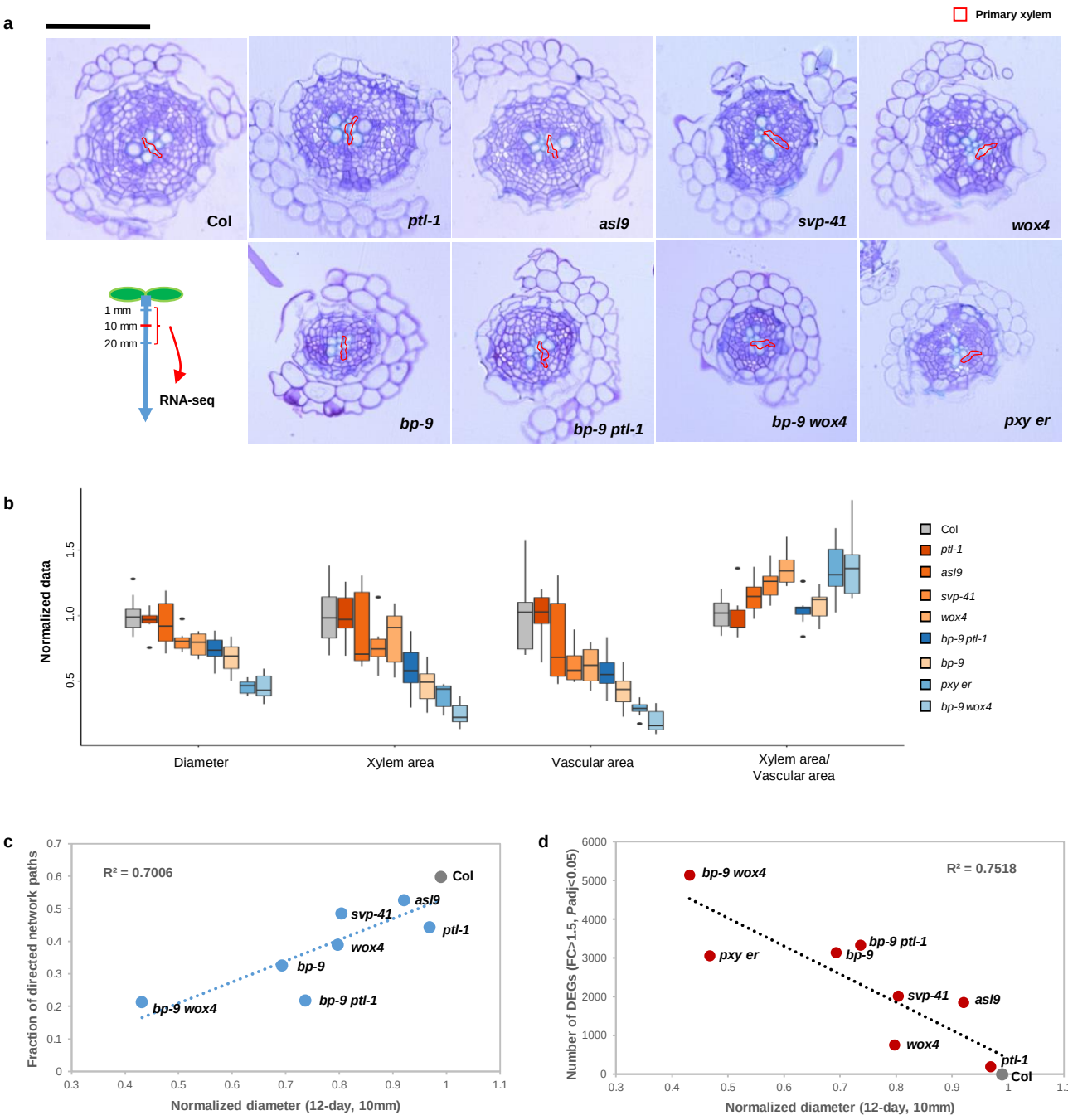

Supplementary Fig. 10 | Genome-wide transcript profiling by RNA-seq in selected mutants.

a, Root fragments undergoing radial growth (1mm - 20mm below root-hypocotyl junction) of 12-day old wild-type (Col) and eight mutants were collected for RNA-Seq experiment. Cross sections were taken at the middle of the root fragment (10mm) from the same batch of plants used for RNA-seq. The primary xylem axis is marked in all lines. Scale bar, 100µm. **b,** Vascular phenotypes including diameter, xylem area, vascular area and proportion of xylem were quantified in the same

batch of sections present in **a**. All measurements were normalized to Col (**Supplementary Table 6c**). Box-and-whisker plots are centred at the median, which splits first and third quartiles. Whiskers show range and black dots represent outliers. **c,** Correlation between the predicted phenotype severities indicated as "Fraction of directed paths measurement" based on the network (**Supplementary Table 3c**) and the vascular diameter in 12-day old Col and mutants. **d,** Correlation between the number of Differentially Expressed Genes (DEGs) and vascular diameter in 12-day old Col and mutants. Linear regression model was adopted and R-squared (R^2) was used to measure the correlation in **c** and **d**. The exact number of independent roots (n) for each line in **b-d** can be found in **Supplementary Table 6c**.

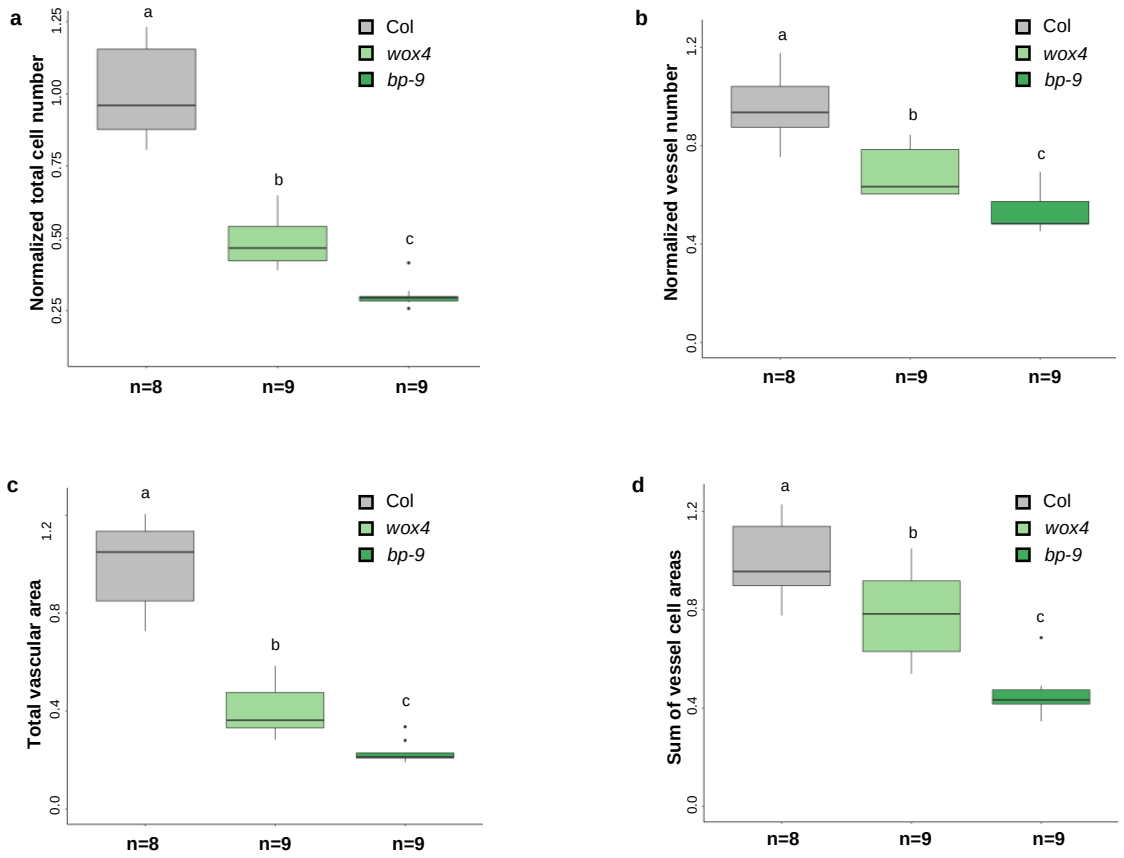

Supplementary Fig. 11 | Phenotypical characterization of *KNAT1* and *WOX4* mutants with LithoGraphX.

a, Total vascular cell numbers of wild-type (Col), *wox4* and *bp-9* were counted using LithoGraphX. **b,** Differentiated vessel numbers of all genotypes were counted using LithoGraphX. **c,** The area of each vascular cell was measured using LithoGraphX and the sum of all vascular cell areas was calculated to obtain the total vascular area. **d,** The area of each differentiated vessel cell was measured and the sum of all vessel cell areas was calculated. All data were normalized to Col. n, independent roots. Box-and-whisker plots are centred at the median, which splits first and third quartiles. Whiskers show range and black dots represent outliers. Different letters indicate a significant difference (P<0.05) based on a one-way ANOVA (**Supplementary Dataset 2c**).

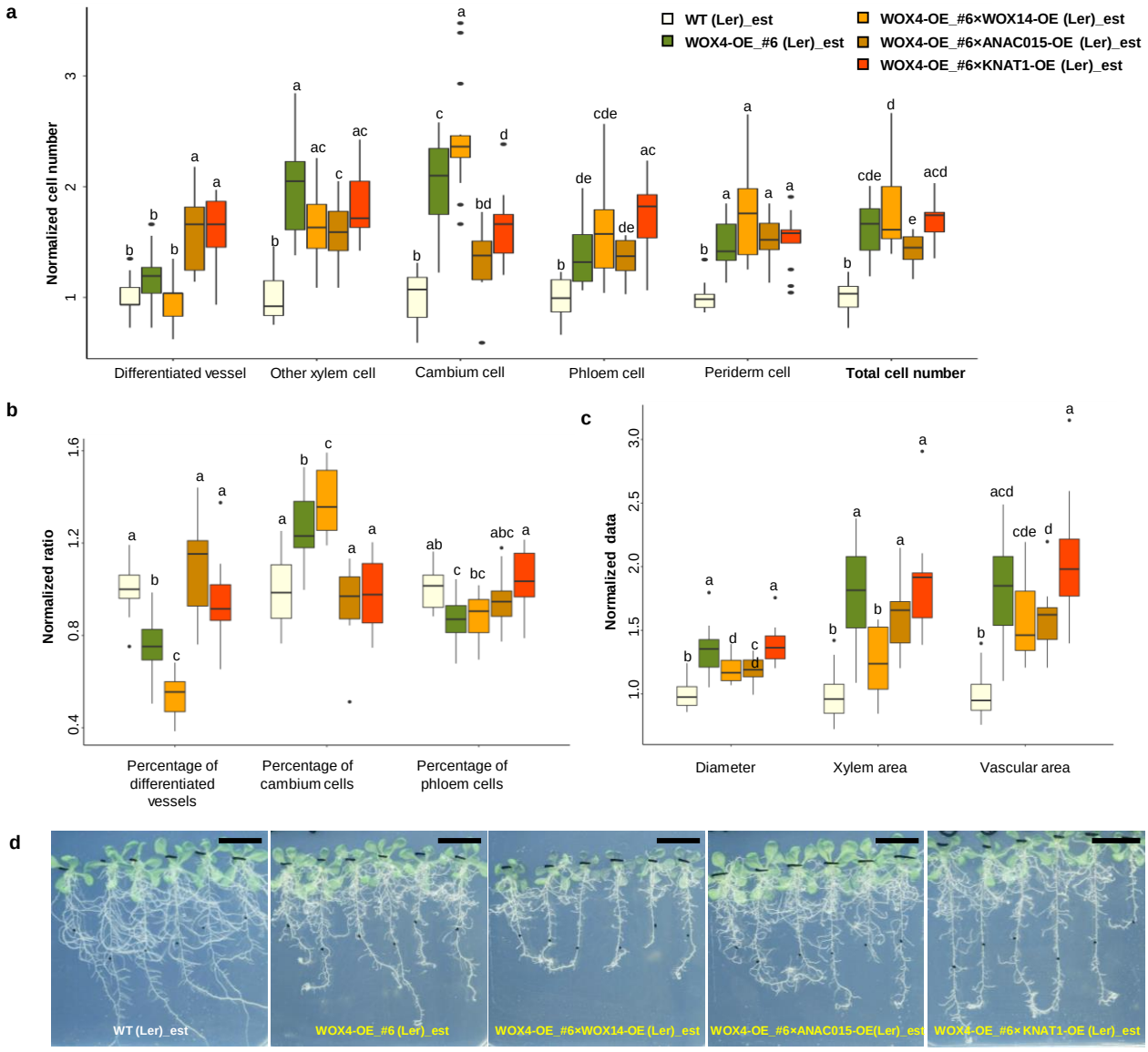

Supplementary Fig. 12 | Synergistic effects of co-overexpressing positive transcriptional regulators on cambial activity and radial growth.

Vascular phenotypes were quantified in wild-type (cambial cell proliferation marker line *pCYCD3,1::GUS* (Ler), marked as WT (Ler)), WOX4 single overexpression (OE) line (#6) and three double OE lines. All lines were treated with 5µM estradiol (est) to induce the expression of target genes for 7 days in 7-day old seedlings. **a**, Five cell types including differentiated vessel, other xylem cell, cambium cell, phloem cell and periderm cell are classified and calculated in one quarter of each cross-section as shown in **Supplementary Fig. 1d** in all lines. **b,** The percentage of

three cell types were calculated in all lines. **c,** Vascular diameter, xylem area and vascular area were measured in all lines. All data were normalized to WT (Ler). Box-and-whisker plots are centred at the median, which splits first and third quartiles. Whiskers show range and Bblack dots represent outliers. Different letters indicate a significant difference ($P<0.05$) based on a one-way ANOVA (the exact *P* value for each comparison can be found in **Supplementary Dataset 2d**). The exact number of independent roots (n) for each line can be found in **Supplementary Table 5b**. Phenotypes were analysed in F1 from two independent crosses with similar results. **d**, The plate images of 14-day old plants treated for 7 days on 5µM est plates in WT (Ler), WOX4-OE and double OE lines. Note the root tip phenotypes in all WOX4-OE lines. The experiment was repeated three times. Scale bars, 2cm.

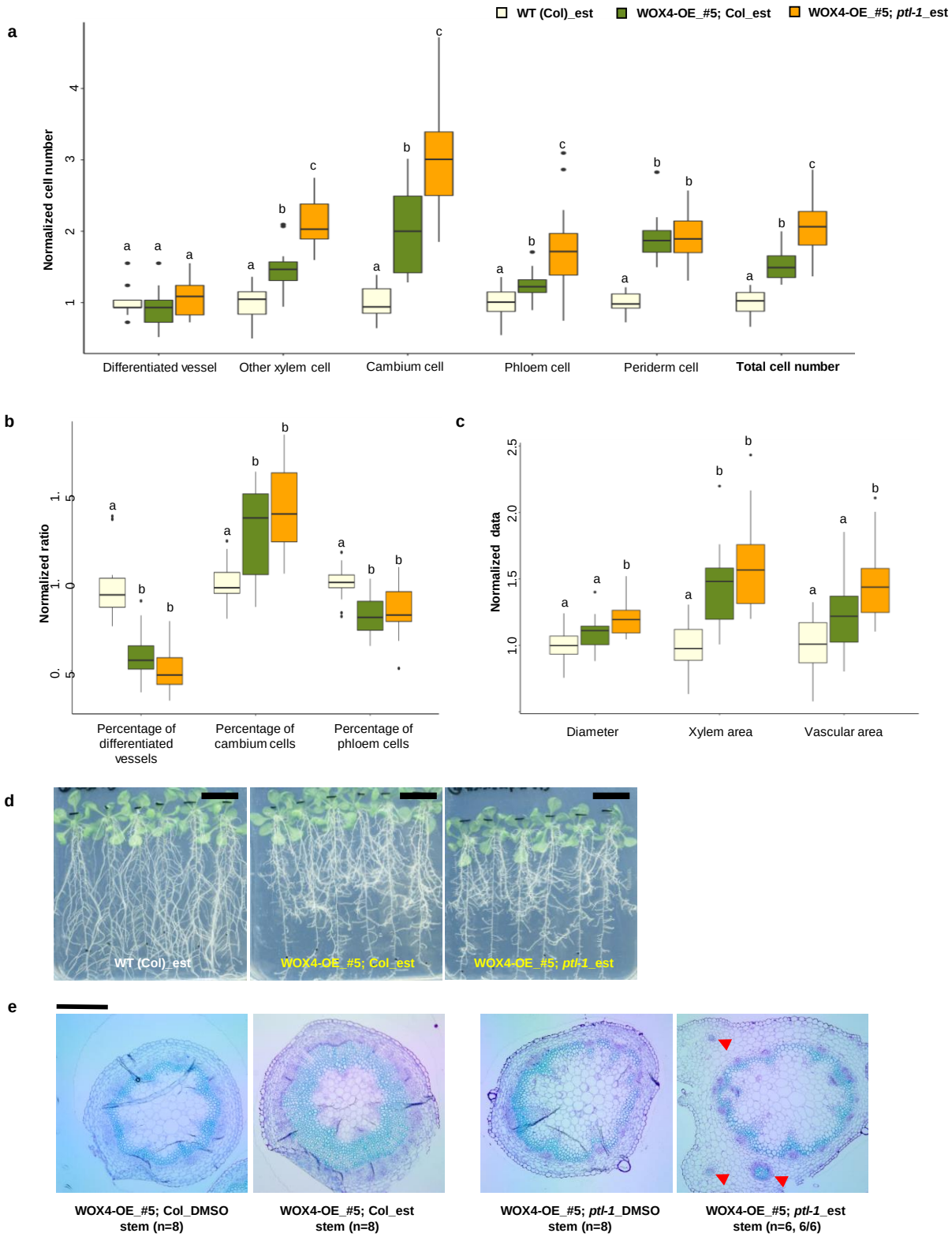

Supplementary Fig. 13 | Removing putative negative regulator *PTL* enhances the effects of overexpressing *WOX4* on cambial activity and radial growth.

Vascular phenotypes were quantified in wild-type (marked as WT (Col)), WOX4-OE in Col (#5,

marked as WOX4-OE_#5; Col) and *ptl-1* background (WOX4-OE_#5; *ptl-1*). **a-d**, All lines were treated with 5μM est to induce the expression of *WOX4* for 7 days in 10-day old seedlings. **a**, Five cell types including differentiated vessel, other xylem cell, cambium cell, phloem cell and periderm cell are classified and calculated in one quarter of each cross-section as shown in **Supplementary Fig. 1d** in all lines. **b,** The percentage of three cell types were calculated in all lines. **c,** Vascular diameter, xylem area and vascular area were measured in all lines. All data were normalized to WT (Col). Box-and-whisker plots are centred at the median, which splits first and third quartiles. Whiskers show range and Bblack dots represent outliers. Different letters indicate a significant difference ($P<0.05$) based on a one-way ANOVA (the exact *P* value for each comparison can be found in **Supplementary Dataset 2e**). The exact number of independent roots (n) for each line can be found in **Supplementary Table 5b**. Phenotypes were analysed in F1 from two independent crosses with similar results. **d**, The plate images of 17-day old plants treated for 10 days on 5μM est plates. Note the root tip phenotypes in WOX4-OE_#5; Col and WOX4-OE_#5; *ptl-1* lines. Scale bars, 2cm. **e**, Ectopic cambium islands were observed in all the stems of WOX4-OE_#5; *ptl-1* after 4-week induction but not in that of WOX4-OE_#5; Col. Sections were taken from the bottom of the main stem. Red arrowheads indicated ectopic cambium islands. All cross sections were stained with Toluidine blue O. All experiments were repeated at least twice. Scale bars, 100μm.

Supplementary Tables 1-8

Supplementary Table 1: Cambium enriched gene and gene module identification in Arabidopsis roots

a, Description of all markers used for cell sorting in Arabidopsis roots. **b,** Normalised transcriptome data of ARR15-expressing cells and other non-overlapping cells in Arabidopsis roots. For each probe, mean value of three biological replicates was shown. **c,** Genes enriched in ARR15-expressing cells (cambium cells) identified by Differentiated expressed genes (DEG) analysis. **d,** Gene regulatory modules with predicted gene members. The number of genes in each module was indicated after the module (M) number; Cambium enriched modules are marked with "*". **e,** Transcription factors (TFs) identified in the cambium enriched modules. **f,** Gene Ontology (GO) enrichment in the cambium enriched modules.

Supplementary Table 2: Identification of cambium transcription factors (TFs)

Gene information and expression patterns of the 41 candidate TFs. Locus (accession number), Description (gene name), TF family, Gene Module and the Source was indicated for each TF. [a]Cambium enriched module (M) was in bold and marked with "*". [b] "The initial cambium TFs" were identified by combination of both Differentiated expressed genes (DEG) analysis and Module analysis (**Fig. 1a**). "Homologues of initial TFs" and a few "cytokinin (CK) induced" TFs were added (**Supplementary Note**). [c]Expression pattern of each TF was investigated with transcriptional GUS reporter and/or RNA *in situ* (**Fig. 1b** and **Supplementary Fig.3**). [1]Cambium TFs: genes that were abundantly expressed in cambium or more broadly expressed in cambium and vascular tissues; [2]Non-cambium expressed TFs: genes that were expressed in tissues other than cambium. N.A., Not Analysed.

Supplementary Table 3: Transcript profiling for network and the mutant phenotype prediction

a, qRT-PCR data used for network construction, i.e, the average fold change from three assays in each inducible overexpression (OE) line. **b,** *P* value for the qRT-PCR data was shown. Unpaired parametric t-test (two-tailed) was used to analyse the data with GraphPad PRISM v.7. **c,** The severity of relevant mutant phenotypes (measured by the "Fraction of directed network paths") was predicted based on the network.

Supplementary Table 4: Plant materials, cloning vectors and primers used in this study

a, Mutation information, source and genotyping primers for the mutant alleles that were used in this study. **b,** Arabidopsis seeds published previously and analysed in this study. **c,** Cloning primers for making entry clones and related vectors constructed in this study. **d,** Primers used to generate the vectors for *in situ* probes. **e,** Primers used in qRT-PCR for network construction.

Supplementary Table 5: Vascular phenotype characterization in overexpression lines

a, Number of independent roots (n) and *P* values (from two-tailed Student's t-test) for vascular phenotype characterization in the single overexpression lines for **Fig. 2a** and **Supplementary Fig. 4b-e**. It was marked as red if *P* value is less than 0.05 compared to the DMSO control. **b,** Number of independent roots (n) analysed in the combinatorial overexpression lines for **Fig. 4** and **Supplementary Figs. 12a-c** and **13a-c**.

Supplementary Table 6: Vascular phenotype characterization of mutants

a, Summary of vascular phenotype characterization of all mutants (17-day) for **Figs. 2c-d**, **3a** and **Supplementary Figs. 5-9**. For each mutant, the total number of independent roots (N), the Experiment numbers, the normalised Medium values of each phenotype and the *P* value (from two-

tailed Student's t-test) for each comparison was shown. *If the significance (*P* value<0.05 compared to the reference genotype) of each phenotype was observed in more than half percentage of the experiments, it was marked as red. #Phenotype category: Mutant with significant changes on "diameter" or "cell count" was marked with orange filling while mutant with significant change only on the ratio of "vessel number/diameter" was labelled with blue filling. Mutants with phenotypes on both categories were indicated with two-colour squares divided diagonally. **b,** Vascular phenotype characterization of mutants (17-day) in each experiment. The number of independent roots (n) in each experiment and the *P* value (from two-tailed Student's t-test) for each comparison was shown. **c,** The exact number of independent roots (n) for each line and vascular phenotype characterization of mutants (12-day) that were used in RNA-seq for **Supplementary Fig. 10**.

Supplementary Table 7: Differentially expressed genes in mutants

a-h, RNA-seq data for Differentially expressed genes (DEGs) in single and double mutants including *ptl-1*(**a**), *asl9* (**b**), *wox4* (**c**), *svp-41*(**d**), *bp-9* (**e**), *bp-9 ptl-1* (**f**), *bp-9 wox4* (**g**) and *pxy er* (**h**). For each gene, the average read count of three experiments was shown for Col and each mutant. Adjusted *P* value (analysed with DESeq, see Methods) was calculated and used to define a DEG. Genes that were overlapped with "Cambium TFs" were listed on the top of the list and highlighted in red.

Supplementary Table 8: Cambium genes are perturbed in mutants

a, The numbers of overlapped genes between Differentiated expressed genes (DEGs) (obtained from **Supplementary Table 7**) and the various gene lists in each mutant were identified using Venn Diagram (Venny 2.1.0). Data were for **Fig. 3b**. **b,** The list of previously reported xylem network genes.

Supplementary Datasets 1-4

Supplementary Dataset 1: Source data for correlation analyses

The predicted phenotype severity (indicated as "Fraction of directed paths measurement") and the experimental data, including Diameter, Cell counts, Vessel number and Vessel number/Diameter for Col and the mutants whose phenotypes were predicted by the cambium transcriptional network. Data were used for the correlation analyses in **Figs. 2d** and **Supplementary Fig. 5**.

Supplementary Dataset 2: ANOVA output data

ANOVA output data, including *P* value for each comparison for **Fig. 3d** (**a**), **Supplementary Fig. 8e** (**b**), **Supplementary Fig. 11a-d** (**c**), **Supplementary Fig. 12a-c** (**d**) and **13a-c** (**e**). It was filled in red if *P* value is less than 0.05.

Supplementary Dataset 3: LithoGraphX Cell classifier raw data

The raw data obtained from LithoGraphX Cell classifier for Col, *wox4* and *bp-9* (see **Fig. 3c-d** and **Supplementary Fig. 11a-d**).

Supplementary Dataset 4: RNA-seq read counts of wild type (Col) and mutants

For each gene, the read counts from individual RNA sample of Col and all mutants were shown.

Zhang_Cambium paper codes

The codes for cambium transcriptional network construction and perturbation analysis, codes and packages for box plots and violin plots generated in this study and the LithoGraphX parameters used in this study. All codes are available on Github (https://github.com/Zhangcambium2019/Zhang2019.